Journal of Sedimentary Research, 2017, v. 87, p. 253-271.

SEASONAL PATTERN IN THE HIGH-ELEVATION FLUVIAL TRAVERTINE FROM THE JIUZHAIGOU NATIONAL NATURE RESERVE, SICHUAN, SOUTHWESTERN CHINA

Stefano Lugli[a], Ya Tang[b], Matteo Reghizzi[a], Xue Qiao[b], B. Charlotte Schreiber[d], Guiping Deng[e]

[a] Dipartimento di Scienze Chimiche e Geologiche, Università degli Studi di Modena e Reggio Emilia, Via Campi 103, 41125 Modena, Italy. Corresponding author: stefano.lugli@unimore.it
[b] Department of Environmental Science, College of Architecture and Environment, Sichuan University, N. 24, South Section One, First Ring Road, Chengdu 610065, Sichuan, China.
[d] Department of Earth and Space Sciences, University of Washington, PO Box 351310, Seattle, WA 98195, USA.
[e] Jiuzhaigou Administrative Bureau, Zhangzha Town, Jiuzhaigou County 623402, Sichuan, China.

ABSTRACT

The Jiuzhaigou National Nature Reserve on the Tibetan Plateau (Sichuan, southwestern China) is characterized by the deposition of fluvial travertine in a spectacular array of shoals, waterfalls, pool dams, and multicolored lakes. This is possibly the highest vegetated travertine setting of the world, from 2200 to 2900 m above sea level, an environment sensitive to minimal changes in temperature and precipitation regime. The evolution of the system is driven by two seasonal monsoon climate patterns with a wet spring-summer travertine deposition and then a dry fall-winter characterized by no precipitation or erosion. Spring and phreatic-vadose deposits transition from laminated columnar calcite to clotted micrite encrustation, possibly correlated with a mid-Holocene peak in precipitation and high lake levels in the Northeastern Tibetan area connected to glacial advance. The most peculiar features are the fluvial shoals, a rather uncommon travertine surface consisting of two main superimposed facies of alternating weak- and strong-turbulence water flow. The low-turbulence facies consists of clotted micrite encrustation of mosses and cyanobacteria filaments, and platy calcite crystals covering algal filaments. The high-water-turbulence facies show seasonal alternation of diatom-rich bundles of *Phormidium* sp. (late spring) with algal *Oocardium stratum* levels (summer-fall). Upslope and downslope of the shoals, the precipitation of calcium carbonate results in the formation of prograding waterfalls and dam-pool systems that encrust macrophytes with microspar and clotted micrite. Encrusted chironomids larvae tubes are present in the waterfall walls up to an elevation of 2860 m, possibly the highest ever recorded. Early diagenetic processes such as dissolution of diatom frustules take place over the span of several years, a slower phenomenon compared to other travertine occurrences. In this high-elevation extreme setting, travertine sand and gravel bar deposits are produced by the exposure to severe weathering of a section of the valley that is bypassed through an underground karst system during the winter dry season.
High-elevation travertine probably has a low preservation potential, but it appears to be more sensitive to climate changes than other depositional settings, especially in the Himalayan-Tibetan area, where the extent of the Quaternary glacial advances and retreats is still a matter of debate.

Keywords: travertine, calcium carbonate, facies analysis, tufa.

INTRODUCTION

The Jiuzhaigou National Nature Reserve is a UNESCO World Natural Heritage site and a Man and Biosphere Reserve located in the Sichuan province of southwestern China. It is considered to be one of the most spectacular natural travertine deposits in the world. It lies in the transitional area from the edges of the humid Sichuan basin extending up to the semiarid Tibetan Plateau. The peculiarity of this site is the deposition of travertine in a high-altitude carbonate-dominated fluvial system that developed from ambient-temperature waters. The strong seasonality of the area induces some variations in the physical, chemical, and biological mechanisms responsible for travertine formation elsewhere in the world (Pedley 1990; Liu et al. 1997; Viles and Pentecost 1999; Wright 2000; Chen et al. 2004; Pentecost 2005; Pedley and Rogerson 2010; Capezzuoli et al. 2014).

Presently travertine is forming at elevations from 2200 to 2650 m. However, until about fifty years ago, when artificial drainage shifted the initiation point downstream, it was precipitating in a section of the valley up to an elevation of 2900 m. Although other examples of even higher-elevation deposition are known, such as Huanglong (3100 to 3600 m above sea level; Zhang *et al*. 2012), the Datong River valley (3815 m, Mischke and Zhang 2008); the Andean Altiplano (3860 m, Valero Garcés *et al*. 2001) and Southern Tibet (4376 m; Zentmeyer et al. 2008), they consist of bare travertine originated by the contribution of deeply sourced CO_2 or hydrothermal fluids. To the best of our knowledge, Jiuzhaigou represents the highest-elevation examples of vegetated, ambient-temperature, fluvial travertine in the world. This because travertine deposition is strongly influenced by temperature and precipitation rate and virtually no deposits exist in areas at a mean annual air temperature below 5°C (Pentecost 1995). As soil respiration increases with rising temperature, more soil CO_2 is available for limestone solution, where sufficient percolation water is available. Higher temperatures enhance carbon dioxide degassing from emerging groundwater and increase aquatic-plant photosynthesis and evaporation, all factors contributing to travertine deposition. The mean annual temperature in Jiuzhaigou is just above the 5° C limit (6.7° C in the period 2000-2007) and, despite the high elevation, soil atmosphere is the most important contributor of carbonic acid leading to limestone dissolution. This is because in the southeastern side of the Tibetan Plateau the alpine tree lines are the highest in the Northern Hemisphere and among the highest worldwide (up to 4850 m above sea level; Miehe *et al*. 2007). The extreme depositional conditions suggest that the system is very sensitive to minimal changes in temperature and/or precipitation regime and may switch to a nonvegetated travertine setting. Moreover, the monsoonal precipitation pattern induces a peculiar depositional seasonality and the severe high-elevation climatic conditions greatly enhance the production of clastic travertine compared to other occurrences elsewhere. It follows that the Jiuzhaiugou travertine may represent a valuable paleoenvironmental archive in an area where the Quaternary climate evolution and glacial history are still under discussion (see Heyman 2014 and Owen and Dortch 2014, for discussion).

Only a few papers have been published on the biological and morphological aspects of the Jiuzhaigou travertine system (Pentecost 2004; Pentecost and Zhang 2000, 2001; Florsheim et al. 2013), but no description of the depositional facies and their evolution is available in the literature. This paper describes the sedimentology and petrography of the Jiuzhaigou fluvial travertine structures in present-day natural deposits, in other recent features, and in controlled precipitation experiments. The goal is to provide the first description of the travertine seasonal patterns that may help in the recognition of ancient high-elevation sequences that are relevant for their paleogeographic and paleoenvironmental significance.

GENERAL SETTING

Jiuzhaigou (‘‘valley of nine villages’’) is located about 400 km north of Chengdu in the Minshan region of northern Sichuan province, on the eastern margin of the Qinghai-Tibetan Plateau, southwestern China (Fig. 1). The Jiuzhaigou area includes two long and narrow valleys, the western Rize valley and the eastern Zezhawa valley, merging into the Shuzheng valley, which finally joins the Baihe River, a tributary to the Yangtze River (Fig. 1). The valleys are fed by numerous springs and form a Y-shaped river system, about 30 km in total length, hosting one of the largest series of travertine-dammed lakes in the world (Pentecost 2005). Within the park there are 118 lakes and pools, 17 waterfalls, 5 shoals, and at least 47 springs (Gu et al. 2013). The active travertine deposition encompasses the area located from the elevation of about 2200 to 2650 m (Fig. 2).

Approximately 60% of the area is covered by pine and deciduous forests in the area below 2900 m altitude. Above 2900 m are subalpine conifer forests with rich biodiversity (Tang 2006).

The valleys fall within a climatic range with a maximum monthly-average air temperature of 16.6° C in July and below 0° C between December and February (minimum is -3.9° C in January). The maximum monthly-average hourly solar radiation spans 248.1-264.7 W/m^2 between May and August. The minimum monthly-average hourly solar radiation of 110.1 W/m^2 is in December. The wet season runs from April to October (68.7-96.8 mm precipitation; the maximum is in August), and the dry season is from November to March (< 35.3 mm precipitation, with a December minimum of 2.5 mm; data from Nuorilang meteorological station, 2000 to 2007). The river water temperature

increases downstream (from 8.3 to 14.8°C in September 2010), with higher values in the lakes (up to 16.7°C at Tiger Lake in September 2010; Florsheim et al. 2013; Fig. 2).

GEOLOGICAL SETTING

The Jiuzhaigou area is located in the Min Shan range, which, together with the Longmen Shan range to the south-west, makes up the mountain front along the eastern edge of the Qinghai-Tibetan plateau. The plateau margin runs at the northwestern side of the Sichuan Basin and is impressively steep: over horizontal distances of 40–60 km, land rises from the western edge of the Sichuan Basin to the west from 500-700 m to over 6000 m elevation (Kirby et al. 2000). The margin was first slowly exhumed during early Cenozoic time and then rose rapidly around 30–25 million years ago and again at 10–15 million years ago up to the present (Wang et al. 2012). The spectacular uplift of the Tibetan plateau that produced the highest mountains in the world began over 50 million years ago as a result of the collision of India with Eurasia, which accommodated at least 1,400 km of north–south crustal shortening (Hubbard and Shaw 2009).

The Min Shan region is characterized by a Paleozoic–Mesozoic sequence, more than 4000 m thick, made up of marine platform, shallow-water siliciclastic rocks and reef-bearing limestones (Kirby et al. 2000). This sedimentary sequence in the northern Min Shan extends to the east with late Proterozoic–Silurian rocks that rest unconformably on metamorphosed Precambrian rocks. The Carboniferous and Permian sequence thins on the platform, and the overlying Triassic rocks shift from shallow-water limestones to thick deep-water flysch deposits typical of the Songpan-Garze basin (Kirby et al. 2000).

The western boundary of the Min Shan range is represented by the Min Jiang reverse-fault zone, which served as an important paleogeographic boundary in the Paleozoic and early Mesozoic (Burchfiel et al. 1995). Another important tectonic feature is the juxtaposition of the Huya fault in Devonian–Triassic siliciclastic and carbonate rocks on the west with the Proterozoic crystalline basement and the cover sequences of the west Qinling orogen to the east.

The Jiuzhaigou Nature Reserve area is characterized by a folded and faulted Devonian to Triassic sedimentary sequence consisting of siliciclastic and carbonate units arranged NW-SE, cut first by a set of faults along the same trend and by a second set approximately perpendicular to it (Fig. 1; Guo et al. 2006).

MATERIALS, METHODS, AND TERMINOLOGY

We carried out a detailed sedimentological and petrographic facies analysis of the most common travertine morphologies of the Jiuzhaigou Reserve using the terminology described in Pentecost and Zhang (2000), Pentecost and Zhang (2001), Pentecost (2004), Pentecost (2005), and Florsheim et al. (2013). The Jiuzhaigou travertine comprises rock types that are named in the English-language literature as calcareous tufa, which applies to soft, porous, poorly consolidated deposits containing plant remains as opposed to dense, layered deposits from hot springs (Pedley 1990). In this paper we use the broader term travertine following the discussion of Pentecost (2005), who recognized that here is no practical way of unambiguously setting a degree of strength or consolidation to these deposits, especially in cases where deposition is not obviously associated with plants. As tufa and travertine would be possibly interlayered or the lateral equivalent one of the other, according to Pentecost (2005): “Not only would it be impracticable to distinguish layers and give them separate names, but it is difficult, if not impossible to determine the precise origins of many ancient travertines”. We used the terminology of Fouke et al. (2000) and Pedley et al. (2003) for the description of spring deposits. For the descriptions of calcite fabric, as seen in thin sections, here we use the terminology: micrite (crystals < 4 μm), microsparite (4 to 10 μm crystals) and sparite (> 10 μm crystals), with no genetic implications.

Travertine crusts being deposited in the river were sampled by cutting with a knife a square 5 cm wide and 3 cm deep in October 2010. The present-day rate of travertine deposition was tested by placing a few flat plastic plates on the bottom of the stream, in order to have an example of a typical yearly rate of deposition. The plastic plates were 10 cm x 15 cm in area and 2 mm thick, and were fixed to the bottom of the stream at Pearl shoal under approximately 20 cm of water from August 2010 to August 2011.

A total of 15 active and 25 recent representative travertine lithologies were sampled for petrographic analysis (7 samples from springs, 5 from shoals, 10 from dam and pools, 10 from waterfalls, 5 from shield caves, 3 of clastic travertine). The travertine samples were impregnated in epoxy resin under vacuum for the preparation of large (4.5 cm x 6 cm) thin sections for examination under the optical polarizing microscope (Leitz and Meiji) in transmitted light using a wide range of magnifications, from 7.5x to 100x. Samples of travertine and host rock were collected in October 2010, July 2011, August 2012, and April and December 2015.
The microstructure of travertine was studied using a field-emission scanning electron microscope (FEG-SEM) FEI Nova NanoSEM™ 450 equipped with QUANTAX EDS Slim-line Technology. Some delicate structures were also observed using an environmental scanning electron microscope (ESEM) Quanta-200 FEI. Both machines are from Università di Modena e Reggio Emilia, Italy.

TRAVERTINE DEPOSITION

The Jiuzhaigou travertine system displays a great variety of depositional morphologies and facies. Dissolution of limestones from the bedrock induces water supersaturation and precipitation of calcium carbonate in springs along and the main stream ("autogenic karst waters"; Pentecost and Zhang 2000). The carbon dioxide (CO_2) incorporated in the water necessary for limestone dissolution comes mainly from soils and the atmosphere (meteogene travertine; Pentecost 2005). A partial source of deep CO_2 cannot be excluded, and, as stated by Pentecost and Zhang (2000), "data are insufficient at present to apply deposition models to this system". Calcium carbonate ($CaCO_3$) precipitation from calcium (Ca^{2+}) and bicarbonate ($2HCO_3^-$) ions dissolved in the water is driven by degassing of CO_2 to the atmosphere following the reaction

$$Ca^{2+} + 2HCO^{3-} \rightarrow CaCO_3 + H_2O + CO_2$$

Travertine deposition and morphologies are governed by changes in channel gradient, valley width, rock falls, debris flow, woody debris, and live hydrophilic trees, plus copious karstic resurgences (Florsheim et al. 2013). All these factors in turn influence CO_2 degassing from the river waters and saturation of $CaCO_3$, producing a spectacular array of dams, lakes, waterfalls, and springs along the riverbed. The morphological evolution of the main Jiuzhaigou travertine bedforms were described in detail by Florsheim et al. 2013. The fluvial travertine deposition appears to be confined only along a limited section of the Rize and Shuzeng valleys, approximately between Arrow Bamboo Lake and Bonsai Shoal (Figs. 1 and 2). As shown by the total-dissolved-solids (TDS) profile of the river water, the travertine deposition is triggered by significant groundwater discharge through a system of karstic resurgences (Figs.1 and 2), most of which are not directly visible. At the beginning of the travertine segment the TDS values increase by ~ 30% (215 ppm) over values farther upstream, where travertine is not forming today (151-161 ppm; Florsheim et al. 2013). According to Guo et al. (2006) the subsurface flow originates mostly from the lakes of the Zechawa valley, located to the northeast of the travertine segment (Fig 1). Because of the karstic flow, which is the main solute source for calcium carbonate precipitation in the Rize Valley, the riverbed of the Zechawa valley is dry for most of the year and the valley itself is completely devoid of travertine deposits.
The present array of travertine deposition was artificially modified in the 1960s with the construction of roads for logging. A large portion of the travertine pool-dam system was cut off and dried out completely in the area downstream of Swan Lake (Fig. 2). As a result, the starting point of calcium carbonate deposition was artificially shifted downstream to its present location at Arrow Bamboo. The travertine depositional pattern is also influenced by a system of sinkholes along the travertine segment, such as between Arrow Bamboo Lake and Five-colored Lake. The result is an underground bypass of the river flow with the complete exposure of more than 1 km of the travertine-encrusted riverbed for several months during the winter dry season (Fig. 2). Because of the high elevation, freeze and thaw enhances travertine degradation resulting in extensive erosion and clastic deposition.

DESCRIPTION OF TRAVERTINE FACIES

Most of the springs in the reserve show no significant travertine deposition as they flow directly into the river or into the lakes. The only exception is the Jialijiage Spring, at the west shore of Rhinoceros Lake (elevation 2350 m). The spring is perched on the valley side at about 10 m above the lake level and presently shows a very limited water flow (less than about 1 l/s). The travertine forms a prograding buildup, less than 2 m high, consisting of an apron and channel, a few ephemeral ponds, and a narrow proximal slope in an area encompassing a few square meters (Fig. 3A). Along the channel and the ponds, travertine is encrusting macrophytes, leaves, and mosses (Fig. 3B). Under the microscope, the travertine consists of clotted calcite micrite alternating with microspar encrusting and incorporating numerous ostracod shells up to 0.6 mm across (Fig. 2C).
Older distal-slope-spring deposits crop out immediately to the north of the vent and consist of laminated carbonate floatstone devoid of macrophyte debris up to 40 cm thick (Fig. 3F and G) overlying a porous clastic travertine layer sealing thick debris-flow deposits (Fig. 3B and E). Petrographic examination of the laminated deposit shows relatively large (up to 0.6 mm) vertically oriented rows of calcite crystals alternating with rows of smaller crystals (up to 0.1 mm; Fig. 3G). Algal filaments and moss remains are rare. Some crystal margins consist of micrite and may indicate the activity of endolithic cyanobacteria (Jones 2010). These older slope deposits cover travertine sand and limestone gravels originated from debris flows. In the upper part of the outcrop, the clasts are cemented by a gravitational cement made of stalactites and pillars (stalactites merged with the corresponding stalagmites), up to 1 cm in diameter and up to 5 cm long, grown at the lower surfaces of large clasts (Fig. 3B). The cement occupies a large part of the void space of the clast-supported gravel framework. Under the optical microscope the cement consists of columnar calcite crystals up to 3 mm in length pointing downward and fanning away from the lower clast surfaces (Fig. 3B, D). The lower part of the gravel deposit shows isopachous cement around the clasts and some horizontal calcite rafts (floe calcite; Pentecost 2005) up to 1 cm thick, cemented to the clast surfaces (Fig. 3E). The vertical span between rafts is up to 2 cm, and they form bridge or ladder structures (Kostecka 1992; Gradzinski et al. 2012), similar to those observed in fractures (Van Noten et al. 2013; Gradzinski et al. 2014).

Interpretation: Paleoflow and Lake Level Indicators

Compared to the present-day deposit, the lack of macrophyte debris of the bare, dense, laminated floatstone may indicate deposition in a much larger water flow than today. The observation that in the old spring deposit the laminae are continuous and not truncated suggests seasonal variations with continuous deposition even during periods of low water flow. Similar laminar travertine alternations have been described by Brasier et al. (2010) in Greece, where deposition occurred under the warm and wet conditions in spring and autumn followed by nondeposition in the arid summer months and a winter hiatus caused by cold conditions. In Jiuzhaigou, where the depositional pattern is dominated by the monsoonal regime, the winter and early spring dry season may have been characterized by periods of nondeposition or much smaller calcite crystals alternating with the large columnar calcite deposited in the April-October wet season. If the hypothesis that the lamination represents annual depositional features is correct, then the rate of depositional would be up to 1 mm/year, which is larger than any rate observed today in the Reserve with the exception of the waterfalls (up to 0.2 mm in Pearl Shoal; see the section on “shoals and fluvial crusts”). A similar laminated facies was described for the mid-Holocene travertine of the Qilian Mountains, located about 400 km to the north, by Mischke and Zhang (2008). Its deposition has been linked to a larger discharge than today during wetter climatic conditions occurring at about 4,000 yr BP. These wet climatic phases, which have been documented in other part of the Tibetan Plateau (Owen and Dortch, 2014), may also be responsible for the thick debris-flow deposits which have been sealed by the laminated spring deposits.
In the lowermost part of the section, the cementation of the limestone gravel by stalactitic gravitational cement suggests degassing of shallow seepage waters under vadose conditions, whereas the isopachous cement and rafts indicate a phreatic environment. The rafts are similar to the paper-thin raft travertine originated at the air–water interface in small pools at Rapolano Terme in Italy (Guo and Riding 1992). No evidence of cumulate sediments consisting of sunken rafts has been observed; the rafts are separated through the vertical sequence and are always cemented to

the clasts, suggesting a progressive drop of the groundwater table. The voids containing the cemented rafts are not completely filled by cement, suggesting again a progressive drop of the groundwater table level instead of simple water-level oscillations, an evolution which is also supported by the abrupt passage between the vadose and phreatic types of cement. Although elevation of travertine deposits along valleys may not be age-dependent, in cases where there is no evidence for long-term fluvial incision the occurrence of spring travertine at different elevations can be considered physical evidence of shifts in the water table and a strong argument for comparing the aquifer recharge in different ages (see discussion in Pedley et al. 2003 and Domínguez-Villar et al. 2011). The described characteristics of the modern and ancient deposits at Jialijiage seem to indicate a decrease of the spring flow. The development of raft structures may also indicate an ancient higher water level of the lake of about 7 m. Although the climate signals may be strongly influenced locally (Li et al. 2016), peak wetness in eastern Tibet and high lake levels in the mid-Holocene were documented in a number of sites in the northeastern Tibetan Plateau (Mischke and Zhang 2008, Wischnewski et al. 2011 and references therein) and are also supported by climatic simulations (see Owen and Dortch 2014, for discussion). In summary, wetter conditions in Jiuzhaigou may account for the bare laminated travertine facies, for the thick debris-flow deposits, and, in turn, a higher Rhino Lake level (present level is 2315 m), as recorded by the transition from phreatic to vadose conditions of the gravel-cementing facies. Other independent analyses are needed to confirm this evolution, but the higher mid-Holocene precipitation regime was possibly recorded in the Jialijiage deposits because the oldest travertine in this area has been dated to 5960 ± 860 and 11290 ± 220 yr BP by Guo et al. 2006.

Pools and Dams

Vegetated pool and dam systems are common features in Jiuzhaigou inasmuch as they cover the largest area of the valley, as in Shuzheng (Fig. 4A), Nourilang, and downstream of the Panda waterfall (see Figs. 1 and 2 for locations). The dams commonly have a vertical wall facing the upstream pool but have a gentle slope downstream (Pentecost 2005). This type of travertine depositional system developed in sections of the valley with a very variable slope. The gentle-slope riverbed where pool and dam travertine is growing today is located immediately downstream of the Shuzheng waterfall, whereas the steepest section formed downstream of Swan Lake and is no longer active (Fig. 2). This dry section of the vegetated dam and pool system, being located at an elevation between approximately 2600 and 2900 m, is probably the highest elevation example in the world. Here the travertine is the most porous, because of the frequent well-preserved molds of stems and leaves (Fig. 4C). No plant remains are visible in the log molds in this location. In the small pool-dam system downstream of the Nuorilang waterfall, the petrography of this lithofacies consists mostly of a delicate framework of very thin, generally less than 0.2 mm, clotted micrite veneers encrusting mosses or growing directly on plant remains. The micrite is in turn overlain by microspar and platy calcite crystals radiating away from the crust and including cyanobacterial filaments, probably *Phormidium* (Fig. 4D). The platy calcite crystals on top of the crust are commonly slightly corroded and are draped by a thin veneer of reddish fine-grained sediment.

Interpretation: Alternation of Wet and Dry Seasons

Lake dams and smaller pool dams may be located on top of primary dams (see below for description), but are present in areas with very different riverbed slope. The pools and dams act as roughness elements causing resistance to water flowing over the downstream side of primary travertine dams (Florsheim et al. 2013). Wood debris and leaves floating in the shallow water are trapped at the upper rim of the dams and become actively encrusted by travertine (Fig. 4B). Wood debris is quickly colonized by mosses, which in turn are encrusted by travertine as well, adding significant volume to the growth of the dam structure. Especially in the high-elevation setting downstream of Swan Lake, organic matter degrades very rapidly. No plant remains were observed in the log molds after the artificial cut-off of this travertine section in the 1960s.

The encrusting mechanism seems to follow a strong seasonal cycle, with the partial drying out of the river flow during the winter. As suggested by the sequence observed under the microscope, the initial incrustation starts with clotted micrite, probably in the low-energy zones of the dam and pool

structures as the spring season floods the system. The precipitation of microspar and platy calcite with *Phormidium* cyanobacteria may follow during the summer directly in the higher-energy areas. With the winter dry season, the microspar and platy calcite at the top of the tiny crust are degraded by frost action and partially covered by fine-grained dust debris. At the beginning of the flooding season in spring the degraded surficial layer is partially eroded away and the erosion surface with its debris filling is then sealed by the new travertine deposition. in this high-elevation setting the winter weathering produces more severe degradation, dissolution, and crumbling phenomena of the dam margins than most other occurrence in the world, especially compared to semiarid (Vazquez-Urbez et al. 2012) and tropical (Carthew et al. 2003) settings, but also to temperate settings (Golubic et al. 2008).

Shoals and Fluvial Crusts

Defined as "broad, gently sloping expanses of turbulent water with rapid travertine deposition" by Pentecost (2005), the shoals seem to be a unique characteristic of the Sichuan region of China (Huanglong and Jiuzhaigou; see also Liu et al. 1995); these large features are not present in other travertine occurrences of the world and are not described in the main models proposed for travertine deposition (Ford and Pedley 1996; Carthew et al. 2003). According to Florsheim et al. (2013), in Jiuzhaigou the shoals are steep, undulating travertine surfaces that appear to be a succession of small, closely spaced, and rounded steps that produce shallow turbulent flow (Fig. 5A). The steps are generally elongated perpendicular to the longitudinal profile but are discontinuous across the channel where the morphology transitions to islands and steps. The height of each step may reach up to ~ 1.0 m in the transition to the downstream waterfall. The shoals may contain vegetated islands or bare travertine.

Two main travertine facies were recognized at Pearl Shoal, one the most spectacular features of the Jiuzhaigou area (Fig. 5A and B, the fluvial crust of Pentecost 2005):

a) Crust colonized by living algae and mosses in low-water-flow turbulence at the rim of the shoal (Fig. 5B); the crust consists of clotted micrite encrusting biological materials such as mosses, algae, cyanobacteria filaments, ostracod shells, and diatom frustules (Fig. 6B).

b) Bare crust with few rare millimeters-long moss stems in the areas of high stream power in the shoal slope (Fig. 5A and C); the last 3 cm of this crust sampled in October 2010 shows an upper part consisting of coalescent subhemispherical structures a few mm across (Fig. 5C). Thin-section analyses show that these features consist of three types of cyanobacterially encrusted laminae alternating with algal structures and vertical sparry calcite lenses; the three cyanobacterial laminae consist of 1) nearly vertically oriented cyanobacterial "bush" fabrics, 2) radiating bundles of *Phormidium* sp. arranged in bush- or shrub-like structures, and 3) vertical calcite crystals arranged in dense laminae including erect parallel filaments of *Phormidium* (very similar to *Phormidium incrustatum* A and B of Freytet and Plet 1996, respectively; Fig. 5B). The three types of cyanobacterial filament-rich laminae alternate with highly porous laminae made of unicellular desmid alga *Oocardium stratum* (Fig. 5B and C). The lower part of the crust at about 2.5 cm depth consists of highly porous clotted micrite and scattered *Oocardium* stratum which encrusted moss stems; filaments of probable *Vaucheria* (an alga belonging to Xanthophyceae) asymmetrically encrusted the downstream side with radial platy calcite crystals (Fig. 6D).

The travertine features resulting from one year's deposition (August 2010 to August 2011) at Pearl Shoal on bare travertine at the margins of the high-turbulence area are revealed by the placement of an experimental plastic plate that became encrusted during that period (Fig. 7A). The crust that formed on the plate was up to 200 µm thick and consists of sparry calcite crystals with sparse *Phormidium* and algal filaments covered by diatom stalks up to 50 µm in length and 10 µm in diameter (Fig. 7B-F; Winsborough and Golubic 1987; Freytet and Verrecchia 1998). In correspondence to the attachment points of the stalk, the crystals show pits on their surfaces (Pedley 2000; Gradzinski 2010). The surface of the plate facing downward and lying in contact with the bed of the stream is coated by a large number of diatoms and EPS (extracellular polymeric substances), which forms a three-dimensional network around the diatom frustules (Fig. 7E). Large diatom frustules are present only on the lower surface of the plate and are completely missing in the top

surface (Fig. 7F). The topmost 2 to 3 mm part of the shoal crusts in both high-energy and low-energy sites contains large quantities of diatoms, but no diatoms are present below the surface.

Interpretation: Transition from Low-Energy to High-Energy Flow

The shoals appear to be produced by the alternation between two different types of crust: the crust colonized by living algae and mosses in low water flow turbulence, and the bare travertine crust produced in high flow turbulence. The bare travertine in the high-energy flow cannot be colonized by moss and algae and is formed by *Phormidium* and *Oocardium* facies, which are not present in the low-energy areas. *Oocardium*, which has been documented in temperate and tropical travertine settings (Pentecost 2005, Golubic et al. 2008), may cope with different flow regimes (Linhart and Schagerl 2015), but it has been documented especially in relatively high-discharge settings ranging from 1 to 10 L/s in Austria (Sanders and Rott 2009), 0.5 to 200 L/s in the British Isles, and 10 L/s in Belgium (Pentecost 1991), and high flow velocities of 2.2–3.5 m/s (Golubic and Marcenko 1958). According to Florsheim et al. (2013) the maximum water speed at Pearl Shoal may reach up to 0.66 m/s. Inasmuch as the one-year precipitation experiment at the margin of the turbulent-flow area produced only one type of crust consisting exclusively of sparry calcite with *Phormidium*, the described facies alternations recovered in the high-stream-power zones may not represent annual lamination, but seem to be related to the switching of the turbulent regime in different areas. These alternations of weak- and strong-turbulence facies appear to be a rather uncommon feature and are probably exclusive of shoal settings. The exceptional width of the shoal itself, which is up to 500 m, and its asymmetric top level are factors contributing to the rapid superimposition of the different flow regimes in adjacent areas. The extent of the observed lamination is also influenced, as a minor effect, by the continuously changing microtopography of the bottom as a result of the relatively high travertine precipitation regime (up to 0.2 mm per year). In recent years the natural switch in the feeding system along the shoal has been partially modified to keep a continuous flow along the whole waterfall front located just downstream of the shoal.

The larger diatom population and diversity and the larger amount of EPS in respect to the upper surface is probably related to conditions of weaker turbulence: although diatoms do withstand high-energy currents (Allan 1995, see the discussion in Gradzinski 2010), they are probably more efficiently attached to substrates of local lower-energy conditions, which in this case are present in the surface oriented downward. This appears to be particularly the case for the largest diatoms (Fig. 7F), which would be more easily swept away by strong currents. The diatom frustules are engulfed by calcite in the crust, but do not seem to represent a direct substrate for nucleation of the crystals (Fig. 7D). The large number of stalked diatoms in the crust being deposited today at Pearl Shoal indicates that, although diatoms do not represent a direct substrate for the growth of calcite crystals, they play a significant role in the framework of the travertine crust by creating widespread microporosity after their dissolution during early diagenesis. These early voids commonly become completely filled by new calcite crystals during later diagenetic stages. Dissolution of the tiny delicate diatom shells may occur within a period of months, or less, in Slovakia and Poland (Gradzinski, 2010). In contrast, at Jiuzhaigou the dissolution of diatoms appears to occur over a longer time period, possibly a few years, as the crust deposited in one year is completely engulfed by diatom frustules (Fig. 7D) and only a few of them show weak early corrosion by dissolution.

The *Oocardium* tubes are not plugged and show no overgrowth of the primary crystallites, suggesting that diagenetic processes did not modify the original structure, phenomena which may occur within months after the growing season in Italy, Croatia (Golubic et al. 1993, Golubic et al. 2008), and Austria (Rott et al. 2012).

Waterfalls (Barrages) and Shield Caves

Waterfalls are located at the downstream edge of primary travertine dams, which are large, well developed travertine structures that extend across the entire valley width at Pearl Shoal, and Norilang, Tiger, Shuzheng, and Bonsai lakes (see Fig. 1 for locations). They show a nearly vertical upstream side, whereas the downstream sides extend across the valley for distances up to 536 m, and heights from crest to base up to 44 m. The waterfalls may be as high as 70 m at Panda Lake and as wide as 300 m at Pearl Shoal Falls, which is 20 m high. The highest waterfalls are located

along faults and lithological changes. Waterfalls normally have irregular wavy patterns along their top edges with protrusions or indentations along the upper margin and large overhangs on the downstream sides that may be subject to mass failure. Eroded blocks of travertine and/or other debris at the base of the falls may reach about two-thirds of total fall height (Florsheim et al. 2013).
The active waterfalls or barrages (Pentecost 2005) cannot be directly examined (Fig. 8A), but the road cut between Swan and Arrow Bamboo lakes (pool and dam system) exposes some older now-dry waterfalls as high as 5 m, revealing their internal structure. Encrusted logs (Fig. 9B) and branches and hanging tree roots represent the core of the main buildup structures, and moss encrustations form the downstream outer wall of the waterfalls. The hanging wall of the medium-size waterfall (a few meters tall) consists of travertine encrustation of mosses fossilized with their stems pointing downward at an angle of 10-20° from the horizontal at the front of the dam (Fig. 9C). Under the optical microscope the cavities formerly occupied by the moss are coated by a thin veneer of microspar up to 0.3 mm thick overlain by an irregular layer of clotted micrite up to 0.4 mm hick (Fig. 8D).
In one site it has been possible to observe small meandering tubes on the vertical downstream wall of a dry waterfall southwest of Swan Lake (Fig. 8E). These tubes are hollow, up to 2 cm long, and up to 1 mm in diameter, with a thin micritic wall (less than 0.05 mm thick) and appear to encrust a clotted micrite travertine containing *Oocardium stratum* structures lying on top of an almost flat moss incrustation (Fig. 8F). The shape and size of these sinuous tubular structures are similar to those described by Gradzinski (2010) in Poland as possible living and feeding burrows of *Chironomidae* (midge) or *Trichoptera* larvae (caddis fly). Similar structures have been described also in Australia (Drysdale 1999), Belgium (Janssen et al. 1999), France (Freytet and Plet 1996), Germany (Durrenfeldt 1978), Greece (Brasier et al. 2011), Japan (Kano et al. 2003), and Italy (Golubic et al. 1993).
The dry waterfalls located in the river segment between Swan and Arrow Bamboo lakes provided the opportunity to also study shield caves formed by the progradation of the hanging top and the lateral margins of the dams. The largest cave is a few meters across and displays on its wall a vertical stratigraphy consisting of large porous moss cushions encrusted by laminated micrite and microspar (Fig. 8C and 9A, B), covered by a dense layer of blocky and interlocked trigonal calcite prisms a few cm thick (Fig. 9D, E and F; Jones and Renaud 2008) in turn covered by a curtain of floatstone consisting of laminated travertine (Fig. 9D). The laminated travertine is cut by an erosional surface and other less distinct surfaces, marked by a film of red-colored fine-grained material, which are in turn covered by new columnar laminitic growth (Fig. 9D). A late dripstone stalactite travertine deposit, up to a few tens of cm across, covers the entire sequence.

Interpretation: the Fast Growing Structures

The waterfalls are the most rapid travertine precipitation sites, inasmuch as physicochemical precipitation and microbial biomediation occur simultaneously (Pedley et al. 2003). The moss incrustation consisting of thin alternating microspar and clotted micrite laminae (Fig. 8D) may be related to deposition during changing seasonal water-flow regimes. The crystallization nuclei are probably provided by the microbial biofilm of cyanobacteria and microscopic chlorophytes. The downward orientation of the moss travertine in the wall of the waterfall is due to the thriving aquatic mosses commonly seen in water spray. The mosses become encrusted by micritic calcite on the stems rather than on actively growing leaflets on the tips, which escape cementation (Golubic et al. 2008).
Surprisingly, the depositional significance of calcium carbonate larval tubes is not negligible even for travertine settings located at an elevation of 2860 m; to the best of our knowledge this is the highest occurrence of these features ever described. The tube structures appear not to be widespread, such as in other temperate and semiarid settings and especially in tropical settings, where calcified caddis-fly nets and retreats may form large parts of the travertine mass and may even provide paleohydrological information (see the discussion in Drysdale et al. 2003). The recognition of the larvae tubes in such a high-elevation setting suggests caution in interpreting the paleoenvironmental conditions of their occurrence in ancient travertine.
The shield caves are created by the rapid horizontal to downward growth of the waterfalls, and the ensuing collapse of the prograding hanging top of the waterfall contributes to the formation of clastic

travertine (Fig. 8A; see next section). The vertical stratigraphy at the wall of the travertine shield cave indicates the transition from conditions of full light exposure (the encrusted moss) to a twilight zone, as the prograding margins and roof of the cave progressively closed in, to the almost aphotic zone within the cave at the last stage of evolution (the laminated travertine). The laminated facies shows columnar projections from the substrate and may have been microbially mediated ("stromatolite-like" tufa; see the discussion in Jones 2010). The erosional truncation of the laminar travertine may represent dissolution of calcitic substrates mediated by microbial biofilms (Jones 2010) or may be related to short exposures of the waterfall system that was subjected to percolation of undersaturated meteoric water, which partially dissolved the cave speleothems. In the dam and waterfall depositional settings a large amount of new encrusting material is added with the "speleomorphization" of the organic remains by the percolation of water through the waterfall structure to form new layered speleothems, as drip-stones (Golubic et al., 1993). This phenomenon occurs also as weak cementation in the clastic travertine gravel and sand.

Clastic Travertine

Downstream of the Panda Lake waterfalls (Fig. 10B and C) we observed travertine sand bars with ripple current structures and gravels consisting of tabular chips of travertine crust up to a few centimeters across (Fig. 10D). Some small recent clastic deposits are weakly cemented into small gravelly bar deposits, which are actively being eroded by the stream flow. Sand-size grains consist of single travertine pustules of *Phormidium*, clotted micrite fragments, carbonate rock fragments, and wood debris (Fig. 10D).

Interpretation: Seasonal Exposure and Erosion of the Riverbed

The clastic travertine is generally produced by a number of processes leading to fragmentation and erosion of previously deposited travertine rocks:
a) collapse of the prograding hanging waterfalls tops, which in Jiuzhaigou created boulders as large as approximately 150 cubic meters at Pearl Shoal Waterfall (Fig. 8A);
b) erosion of travertine at the river floor by channelized and concentrated flow during the dry-season low water level (Fig. 10E);
c) erosion due to increased water level and stream power during floods, as was directly witnessed during August 2012 (Fig. 10C);
d) weathering and disaggregation of the travertine deposits as they become exposed in abandoned river channels, which may subsequently become reactivated again.
The weathering and erosion of travertine, which normally may not produce a significant amount of clastic in other travertine occurrences in the world, appears to happen on a large scale systematically every year between Arrow Bamboo Lake and Panda Lake. This is because the stream water flows underground below the travertine-encrusted riverbed (fluvial crust of Pentecost 2005) for several months (Figs. 1 and 2). The underground bypass of the river section is due to a system of sinkholes located upstream of Panda Lake with resurgence directly within Five-colored Lake. During the dry season the entire reduced water flow is swallowed underground, whereas in the wet season the riverbed act as a large spillover in respect to the sinkhole area. The exposure of the riverbed crust happens between December and May (Fig. 10A), and in winter the disaggregation action of frost is particularly severe on the hanging walls of the Panda waterfall (Fig. 10B). The large amount of travertine clasts derived in these ways is then transported downstream at the next spring flood (Fig. 10C) and accumulates mostly in longitudinal bars (Fig. 10D) at low-energy-flow areas such as depressions, ponds, and around obstacles.

DISCUSSION

Peculiar Depositional Seasonality: Temperature, Water Turbulence, Dryness

Although a clear seasonal sequence of travertine textures may not be necessarily expected, given that local factors greatly influence the depositional array (as discussed by Gradzinsky 2010), a number of sedimentary features observed in the Jiuzhaigou travertine provide indications about

unique seasonal depositional patterns, which are possibly exacerbated by the high-elevation setting of this vegetated system. These sedimentary features are mainly the result of variations in temperature and water turbulence and the desiccation of some areas during the dry season. In Poland, travertine with clotted micrite deposition and abundant diatoms appears to be common in winter settings of low stream energy and splash, while encrusted bacterial filaments are more common during the beginning of the wet season in summer and algal structures are more abundant in the summer wet season in high-energy environments (Gradzinski 2010). In Austrian streams, where the dynamics of the *Oocardium* colonies have been studied in detail (Sanders and Rott 2009, Rott et al. 2012), diatoms are the dominant component in temperate rivers during the cold season followed by an increased contribution of green algae during summer (Linhart and Schagerl 2015). Before leaves shoot and after leaves fall (spring and autumn), the microphytobenthos is dominant because of increased irradiance, suggesting that total algae biomass is driven mainly by light supply, while water temperature controls the general composition (Linhart and Schagerl 2015). Pearl Shoal is such a broad platform at the bottom of a north-south oriented valley that the seasonal effect of solar irradiation is less effective than elsewhere. Here the transition from clotted micrite encrusting moss and shrub-like cyanobacterial structures to algae-dominated *Oocardium stratum* and dense laminae of *Phormidium* suggests a change from relatively low energy deposition to the strong-turbulence regime of the present-day setting. This change in facies association appears to record the episodic shift of the main channels feeding the shoal. The discontinuous laminae consisting of vertical sparry calcite may represent a sort of transition to the stronger-turbulence regime. Moreover, as revealed by the crust that is being deposited today, the peculiar high-frequency alternation between the compact *Phormidium* sparite and the *Oocardium stratum* laminae seem to mark the transition between the late-spring end of the dry season (April) and the more active deposition during summer and fall (May-October), respectively. *Oocardium stratum* seems to carry a specific hydrodynamic significance in this high-elevation setting, in that its occurrence appears to be confined in the very-strong-turbulence zone such as the shoals and falls.

The unique seasonal alternation at Jiuzhaigou is supported by the stratigraphy of the insect larval tubes in the travertine. As water flow and warmth are probably the primary controls on larval abundance (Brasier et al. 2011) and the larval tubes could be considered the best indicator of springtime deposition (Janssen et al., 1999, Brasier et al. 2011). According to Gradzinski (2010), although the tubes are most common at the turn of spring to summer, they cannot be considered an unequivocal marker because they were observed in Poland on travertine grown in June-October and November-March. In Jiuzhaigou instead, the construction of the chironomids tubes is probably related to mid- to late-spring warming of waters, as adult insects leave the tubes during the warmest air temperatures in summer. The water temperature at Pearl Shoal was as high as 11.8-14.0 °C in August 2011. Abundant living caddis-fly larvae with case square in cross section (different from those forming carbonate tubes) were observed attached to obstacles in the high-energy stream at Pearl Shoal at the beginning of April 2015, while in December 2015 only a few were present. If the hypothesis of spring-summer growth of the larval tubes is correct, then the *Oocardium*-rich facies that grew directly on the tubes may actually represent the depositional facies of the declining summer season.

Recognition of High-Elevation Travertines: Criteria and Implications

Inasmuch as the understanding of ancient geographies is a key factor in reconstruction of past climates, recognition of high-elevation vegetated travertine depositional settings appears to be significant for paleogeographic and paleoclimate studies. Our study suggests that vegetated travertine systems are not exclusive of temperate climate settings but may be present also at elevations as high as 2900 m, a setting which is normally dominated by bare travertine. The high-elevation vegetated travertine facies association does not differ significantly from other occurrences at lower elevations, with the exception of a relatively low depositional rate compared to other climate settings and slower diagenetic changes. The depositional rate of 0.2 mm/y that we measured at Peal Shoal is much lower than comparable ramp facies in lower-elevation settings, which are up to 5.20 mm/y at about 1200 m elevation (Arenas et al. 2015) and 18.27 mm/y at about 900 m elevation (Auqué et al. 2014) in the continental Mediterranean climate of Spain. Other direct precipitation yielded a 1.5-3 mm-thick crust in 10 months at about 500 m elevation in temperate Germany (Arp et

al. 2001) and 1.5-2.5 mm/y at about 300 m elevation in humid subtropical Japan (Kano et al. 2003). These direct precipitation data indicate that lamination in the high vegetated travertine is characterized by thinner lamination than in other occurrences. In general, the relatively limited depositional rate is probably the result of lower summer temperature and and long dry season with no deposition in winter-early spring. In the case of Jiuzhaigou, the monsoonal summer season is also characterized by high discharge (up to 9 m^3/s in 2015), a factor which may also reduce travertine deposition because of dilution during high-rainfall periods, as observed for the bare travertine in Huanglong (Zhang et al. 2012). These limiting factors are probably influencing also diagenesis, which appears to proceed at a much slower pace than in any other setting.

At an even higher elevation (> 3000 m), where bare travertine forms (Huanglong, the Andes, and the Himalaya), the limiting effect of low temperature is probably partially balanced by the large endogenic CO_2 flux and/or hydrothermal activity, which enhance carbonate dissolution by groundwater and hence travertine precipitation along springs and streams. These controlling factors are largely independent of climate, and this implies that bare travertine is less sensitive in recording climate changes than the high-elevation vegetated travertine.

Although the preservation potential of high-elevation travertine may be relatively low because of destruction by erosion and glacial action, the study of the vegetated systems carries a particular significance as these systems appear to be mostly the product of wetter and warmer climatic phases, such as the interglacial stages in the Quaternary (Pentecost 1995, Ordoñez et al. 2005, Ortiz et al. 2009). Because the glacial advances in the Tibetan region have been linked to increased monsoon precipitation, cloudiness, and summer cooling in the mid-Holocene (Owen and Dortch 2014), it follows that the intercalation of vegetated and bare travertine facies can be used as a proxy for the glacial history of the area. Multiple Quaternary glaciations with expanded valley glaciers, ice fields, and ice caps have been recorded in Tibet, and at least four general glacial advances and retreats are suggested for the Holocene (Owen and Dortch 2014). The latest of these phases of increased precipitation has possibly been recorded by the deposition of the bare facies that we have discovered at the Jialijiage spring below the present-day vegetated travertine deposits. These considerations imply that the study of vegetated travertine may provide new insights into the glacial evolution of the Himalayan-Tibetan region, an area which is not easy to study, largely because of physical inaccessibility. After the presence of an extensive ice sheet during the global last glacial maximum was postulated (Kuhle 2004, and references therein), geomorphological observations and cosmogenic-exposure dating of glacial landforms (Heyman 2014; Owen and Dortch, 2014 and references therein) have shown that during the last glacial cycles there was no plateau-wide Tibetan ice sheet. As much work is still needed to unravel regional variations of glacial chronologies in the Tibetan area (Heyman 2014), the notion that some travertine at Jiuzhaigou is as old as 21080 ± 580 years (^{14}C dating by Guo et al. 2006), an age close to the peak of the last glacial maximum, seems to support the hypothesis of a limited extent of the glacial advances in the Quaternary.

CONCLUSION

The sedimentology and petrography of the recent and present-day fluvial travertine at Jiuzhaigou indicates some peculiar depositional patterns that develop in the possibly highest-elevation vegetated setting in the world. These patterns are similar to those developing in the temperate regions, but appear to be more sensitive to small changes in temperature and flow regime and may help in recognizing high-elevation travertine in the rock record. One of these changes was recorded by the Jialijiage spring deposits showing a phase of much larger water flow than today. This phase may be related to a hydroclimatic regime shift that occurred in the area in the mid-Holocene and was also coupled by a higher level of the Rhino Lake.

Other major differences are mostly related to the monsoonal precipitation regime and the more severe travertine degradation. As opposed to most temperate travertine settings elsewhere, the dry season is in winter, when the colder temperature further reduces travertine precipitation and diagenesis. The spring flooding season produces erosion followed by most travertine deposition concentrated in spring, summer, and fall.

The recent evolution of the most peculiar features, the shoals, is characterized by the superimposition of two main depositional facies in water flow of weak and strong turbulence. The weak-turbulence travertine consists of clotted micrite encrustation associated with mosses and

cyanobacteria filaments, and radial platy calcite crystals covering algal filaments. The strong-water turbulence lithofacies shows unique seasonal alternation of diatom-rich radiating bundles of *Phormidium* sp. (late-spring end of the dry season) and laminae of vertical calcite crystals with erect filaments of *Phormidium* with highly porous laminae of *Oocardium stratum* (high water during summer and through the fall). These findings indicate that *Oocardium stratum* is colonizing the extreme-turbulence zones during high water level.

The main travertine-built structures are prograding waterfalls and dam-pool systems where encrusted logs, branches, and tree roots form the core of the main dam structures and moss encrustations by microspar and clotted micrite that form the downstream wall of the waterfalls. Adding to the volume of the prograding waterfall are also larval tubes of chironomids, which may represent the highest-elevation occurrence in the world (2860 m). This is also relevant for the biosedimentary and paleoenvironmental reconstruction of fossil travertine sequences, in that these biostructures are most common in temperate and tropical areas (Janssen et al. 1999; Freytet and Plet 1996; Brasier et al. 2011; Drysdale et al. 2003). In such a high-elevation setting, winter weathering produces more severe degradation, dissolution, and crumbling phenomena. Early diagenesis of present-day and recent travertine crusts proceeds more slowly than elsewhere, and one of the most important porosity enhancers, the dissolution of diatom frustules, appears to be negligible, at least on a one-year basis.

The rapid growth and collapse of the hanging wall of waterfalls but especially the karst-induced exposure of long sections of the valley during the severe winter season produce a large amount of clastic travertine, such as sand and gravel bar deposits in the upper reaches of the system, especially during the flooding season in spring.

Although the preservation potential of high-elevation travertine may be relatively low because of erosion and glacial action, the study of these types of deposits may provide significant paleogeographic and paleoenvironmental information, inasmuch as they appear to be more sensitive to climate changes than the bare travertine and the low-elevation depositional settings. This is particularly relevant for the Holocene of the Himalayan-Tibetan area, where the extent of the Quaternary glacial evolution is still under discussion. The preservation at Jiuzhaigou of fluvial travertine as old as about 21000 yr and its facies evolution, which records at least one increased-discharge phase marked by bare travertine possibly connected to the latest glacial advance, seem to provide further clues for a relatively low extent of glacial advances and retreats during and after the last glacial maximum.

7. Acknowledgments

This paper would not have been possible without the kind help and scientific support from the staff of the Jiuzhaigou National Nature Reserve. We thank two anonymous reviewers and editors L. Melim and K.C. Benison for the constructive comments.

8. References

Allan, J.D., 1995, Stream Ecology: Structure and Function of Running Waters. London, Chapman & Hall, 388 p.

Arenas, C., Auqué, L., Osácar, C., Sancho, C., Lozano, M.V., Vázquez-Urbez, M., and Pardo, G., 2015, Current tufa sedimentation in a high discharge river: a comparison with other synchronous tufa records in the Iberian Range (Spain): Sedimentary Geology, v. 325, p. 132-157.

Auqué, L., Arenas, C., Osácar, C., Pardo, G., Sancho, C., and Vázquez-Urbez, M., 2014, Current tufa sedimentation in a changing-slope valley: the River Añamaza (Iberian Range, NE Spain): Sedimentary Geology, v. 303, p. 26–48.

Burchfiel, B.C., Chen, Z., Liu, Y., and Royden, L.H., 1995, Tectonics of the Longmen Shan and adjacent regions: International Geological Review v. 37, p. 661– 735.

Brasier, A.T., Andrews, J.E., and Kendall, A.C., 2011, Diagenesis or dire genesis? The origin of columnar spar in tufa stromatolites of central Greece and the role of chironomid larvae: Sedimentology, v. 58, p. 1283–1302.

Capezzuoli, E., Gandin, A., and Pedley, M., 2014, Decoding tufa and travertine (fresh water carbonates) in the sedimentary record: the state of the art: Sedimentology, v. 61, p. 1–21.

Carthew, K.D., Taylor, M.P., and Drysdale, R.N., 2003, Are current models of tufa sedimentary environments applicable to tropical systems? A case study from the Gregory River: Sedimentary Geology, v. 162, p. 199–218.

Chen, J., Zhang, D.D., Wang, S., Xiao, T., and Huang, R., 2004, Factors controlling tufa deposition in natural waters and waterfall sites: Sedimentary Geology, v. 166, p. 353–366.

Domínguez-Villar, D., Vázquez-Navarro, J., Cheng, H., and Edwards, L., 2011, Freshwater tufa record from Spain supports evidence for the past interglacial being wetter than the Holocene in Mediterranean region: Global and Planetary Change, v. 77, p. 129-141.

Drysdale, R. N., 1999, The sedimentological significance of hydropsychid caddis-fly larvae (order: Trichoptera) in travertine-depositing stream: Louie Creek, northwest Queensland, Australia: Journal of Sedimentary Research, v. 69, p. 145–150.

Drysdale, R.N., Carthew, K.D., and Taylor, M.P., 2003, Larval caddis-fly nets and retreats: a unique biosedimentary paleocurrent indicator for fossil tufa deposits: Sedimentary Geology, v. 161, p. 207–215.

Dürrenfeldt, A., 1978, Untersuchungen zur Besiedlungsbiologie von Kalktuff–faunistische, ökologische und elektronenmikroskopische Befunde: Archiv für Hydrobiologie, Supplementband, v. 54, p. 1–79.

Florsheim, J.L., Ustin, S.L., Tang, Y., Di, B., Huang, C., Qiao, X., Peng, H., Zhang, M., and Cai, Y., 2013, Basin-scale and travertine dam-scale controls on fluvial travertine, Jiuzhaigou, southwestern China: Geomorphology, v. 180-181, p. 267-280.

Ford, T.D. and Pedley, M., 1996, A review of the tufa and travertine deposits of the World: Earth Science Review, v. 41, p. 117–175.

Fouke, B.W., Farmer, J.D., Des Marais, D.J., Pratt, L., Sturchio, N.C., Burns, P.C., and Discipulo, M.K., 2000, Depositional Facies and Aqueous-Solid Geochemistry of Travertine-Depositing Hot Springs (Angel Terrace, Mammoth Hot Springs, Yellowstone National Park, U.S.A.): Journal of Sedimentary Research, v. 70, p. 265-285.

Freytet, P., and Plet, A., 1996, Modern freshwater microbial carbonates: The Phormidium stromatolites of southeastern Burgundy (Paris Basin, France): Facies, v. 34, p. 219–238.

Freytet, P., and Verrecchia, E.P., 1998, Freshwater organisms that build stromatolites: a synopsis of biocrystallization by prokaryotic and eukaryotic algae: Sedimentology, v. 45, p. 535–563.

Gaulke, L.S., Weiyang, X., Scanlon, A., Henck, A., and Hinckley, T., 2010, Evaluation criteria for implementation of a sustainable sanitation and wastewater treatment system at Jiuzhaigou National Park, Sichuan Province, China: Environmental Management, v. 45, p. 93–104.

Golubic, S., and Marcenko, E., 1958, Zur Morphologie und Taxonomie der Desmidiaceengattung Oocardium: Aquatic Sciences: Research Across Boundaries, v. 20, p. 177–185.

Golubic, S., Violante, C., Ferreri, V., and D'Argenio, B., 1993, Algal control and early diagenesis in Quaternary travertine formation (Rocchetta a Volturno, Central Apennines), *in* Barattolo, F., ed., Studies on Fossil Benthic Algae: Bollettino della Società Paleontologica Italina, Special volume 1, p. 231–247.

Golubic, S., Violante, C., Plenkovic-Moraj, A.,and Grgasovic, T., 2008, Travertines and calcareous tufa deposits: an insight into diagenesis: Geologia Croatica, v. 61, p. 363–378.

Gradzinski, M., 2010, Factors controlling growth of modern tufa: results of a field experiment, *in* Pedley, H.M., and Rogerson, M., eds., Tufas and Speleothems: Unravelling the Microbial and Physical Controls: Geological Society of London, Special Publication 336, p. 143–191.

Gradzinski, M., Dulinski, M., Hercman, H., Gorny, A., and Przybyszowski, S., 2012. Peculiar calcite speleothems filling fissures in sandstones and their palaeohydrological and palaeoclimatic significance: example from the Polish Carpathians: Geological Quarterly, v. 56, p. 711–732.

Gradzinski, M., Wroblewski, W., Dulinski, M., and Hercman, H., 2014, Earthquake-affected development of a travertine ridge: Sedimentology, v. 61, p. 238–263.

Gu, Y., Du, J., Tang, Y., Qiao, X., Bossard, C., and Deng, G., 2013, Challenges for sustainable tourism at the Jiuzhaigou World Natural Heritage site in western China: Natural Resources Forum, v. 37, p. 103-112.

Guo, J., Yang, G., Cao, J., Chen, B., Song, Y., Zhang, H., Lu, Z., Cai, Y., and An, D., 2006, Report on the geological environments in the Jiuzhaigou-Huanglong scenic areas: Geological Environment Survey Special Report. Sichuan Bureau of Geology and Mineral Exploration and Development (in Chinese), 191 p.

Guo, L., and Riding, R., 1992, Aragonite laminae in hot water travertine, Rapolano Terme, Italy: Sedimentology, v. 39, p. 1067–1079.

Heyman. J., 2014, Paleoglaciation of the Tibetan Plateau and surrounding mountains based on exposure ages and ELA depression estimates: Quaternary Science Reviews, v. 91, p. 30-41.

Hubbard, J., and Shaw, J.H., 2009, Uplift of the Longmen Shan and Tibetan plateau, and the 2008 Wenchuan (m = 7.9) earthquake: Nature, v. 458, p. 194-197.

Li J., Ehlers T.A., Werner M., Mutz S.G., Steger C., and Paeth H., 2016, Late quaternary climate, precipitation $\delta^{18}O$, and Indian monsoon variations over the Tibetan Plateau: Earth and Planetary Science Letters, v. 457, p. 412–422.

Mischke, S., and Zhang, C., 2008, A laminated tufa carbonate from the mid Holocene of the Qilian Mountains and its potential for palaeoclimate inferences: Episodes, v. 31, p. 401-407.

Janssen, A., Swennen, R., Podoor, N., and Keppen, E., 1999, Biological and diagenetic influence in Recent and fossil tufa deposits from Belgium: Sedimentary Geology, v. 126, p. 75–95.

Jones, B., 2010, Microbes in caves: agents of calcite corrosion and precipitation, *in* Pedley, H.M., and Rogerson, M., eds., Tufas and Speleothems: Unravelling the Microbial and Physical Controls: Geological Society of London, Special Publication 336, p. 7-30.

Jones, B., and Renaut, R.W., 2008, Cyclic development of large, complex, calcite dendrite crystals in the Clinton travertine, Interior British Columbia, Canada: Sedimentary Geology, v. 203, p. 17–35.

Kano, A., Matsuoka, J., Kojo, T., and Fujii, H., 2003, Origin of annual lamination in tufa deposits,southwest Japan. Palaeogeography, Palaeoclimatology, Palaeoecology, v. 191, p. 243–262.

Kirby, E., Whipple, K.X., Burchfiel, B.C., Tang, W., Berger, G., Sun, Z., and Chen, Z., 2000, Neotectonics of the Min Shan, China: Implications for mechanisms driving Quaternary deformation along the eastern margin of the Tibetan Plateau: Geological Society of America, Bullettin, v. 112, p. 375– 393.

Kostecka, A., 1992, Calcite from the Quaternary spring waters at Tylicz, Krynica, Polish Carpathians: Sedimentology, v. 40, p. 27-39.

Kuhle, M., 2004, The high glacial (last ice age and LGM) ice cover in high and central Asia, *in* Ehlers, J., and Gibbard, P.L., eds., Quaternary Glaciations Extent and Chronology, Part III: South America, Asia, Africa, Australia, Antarctica. Amsterdam, Elsevier, p. 175-199.

Linhart, C., and Schagerl, M., 2015, Seasonal succession of the travertine-forming desmid Oocardium stratum: Journal of Phycology, v. 51, p. 1055–1065.

Liu, Z., Svensson, U., Dreybrodt, W., Yuan, D., and Buhmann, D., 1995, Hydrodynamic control of inorganic calcite precipitation in Huanglong Ravine, China: Field measurements and theoretical prediction of deposition rates: Geochimica et Cosmochimica Acta, v. 59, p. 3087–3097.

Liu, Z., Yuan, D., and He, S., 1997, Stable carbon isotope geochemical and hydrochemical features in the system of carbonate-H_2OCO_2 and their implications-evidence from several typical karst areas of China: Acta Geologica Sinica, v. 71, p. 446–454.

Miehe, G., Miehe, S., Vogel, J., Co, S., and La, D., 2007, Highest treeline in the Northern Hemisphere found in southern Tibet: Mountain Research and Development, v. 27, p. 169-173.

Ordoñez, S., Gonzàlez Martìn, J.A., Garcìa del Cura, M.A., and Pedley, H.M., 2005, Temperate and semi-arid tufas in the Pleistocene to Recent fluvial barrage system in the Mediterranean area: the Ruidera Lakes Natural Park (central Spain): Geomorphology, v. 69, p. 332–350.

Ortiz, J.E., Torres, T., Delgado, A., Reyes, E., and Dìaz-Bautista, A., 2009, A review of the Tagus river tufa deposits (central Spain): age and palaeoenvironmental record: Quaternary Science Reviews, v. 28, p. 947–963.

Owen, L.A., and Dortch J.M., 2014, Nature and timing of Quaternary glaciation in the Himalayan-Tibetan Orogeny: Quaternary Science Review, v. 88, p. 14-54.

Pedley, H.M., 1990, Classification and environmental models of cool freshwater tufas: Sedimentary Geology, v. 68, p. 143–154.

Pedley, M., 2000, Ambient temperature freshwater microbial tufas, *in* Riding, R.E., Awramik, S.M. eds., Microbial Sediments: Berlin, Springer, p. 179–186.

Pedley, M., González Martín, J.A., Ordoñez, S., and García del Cura, M.A., 2003, Sedimentology of Quaternary perched springline and paludal tufas: criteria for recognition, with examples from Guadalajara Province, Spain: Sedimentology, v. 50, p. 23–44.

Pedley H.M., and Rogerson M., 2010, In vitro investigations of the impact of different temperature and flow velocity conditions on tufa microfabric, *in* Pedley, H.M., and Rogerson, M., eds., Tufas and Speleothems: Unravelling the Microbial and Physical Controls: Geological Society of London, Special Publication 336, p. 193-210.

Pentecost, A., 1991, A new and interesting site for the calcite-encrusted desmid *Oocardium stratum* Naeg. in the British Isles: British Phycological Journal, v. 26, p. 297–301.

Pentecost, A., 1995, The Quaternary travertine deposits of Europe and Asia Minor: Quaternary Science Reviews, v.14, p. 1005–1028.
Pentecost, A., 2005, Travertine: Berlin, Springer, 445 p.

Pentecost, A., and Zhang, Z., 2000, The travertine flora of Jiuzhaigou and Munigou, China and its relationship to calcium carbonate deposition: Cave and Karst Science, v. 27, p. 71-78.

Pentecost, A., and Zhang, Z., 2001, A review of Chinese travertine: Cave and Karst Science, v. 28, p. 15-28.

Pentecost, A., 2004, Huanglong and Jiuzhaigou, China, *in* Gunn, J., ed., Encyclopedia of Caves and Karst Science, p. 913-916.

Rott, E., Hotzy, R., Cantonati, M., and Sanders, D., 2012, Calcificationtypes of *Oocardium stratum* Nägeli and microhabitat conditions in springs of the Alps: Freshwater Science, v. 31, p. 610–24.

Sanders, D., and Rott, E., 2009, Contrasting styles of calcification by the micro-alga *Oocardium stratum* Naegeli 1849 (Zygnematophyceae) in two limestone-precipitating spring creeks of the Alps *Oocardium stratum*: Austrian Journal of Earth Science: v. 102, p. 34–49.

Tang, Y., 2006, Introduction of Sichuan University and Jiuzhaigou National Park and a proposal for a UCD and SCU research workshop on ecological and environmental sustainability of Jiuzhaigou Park: Executive Jiuzhaigou International Laboratory for Ecology, Environment and Sustainability, Sichuan University, 5 p.

Valero Garcés, B.L., Arenas, C., and Delgado-Huertas, A., 2001, Depositional environments of Quaternary lacustrine travertines and stromatolites from high altitude, Andean lakes, N.W. Argentina: Canadian Journal of Earth Sciences, v. 38, p. 1263-1283.

Van Noten, K., Claes, H., Soete, J., Foubert, A., Özkul, M., and Swennen, R., 2013, Fracture networks and strike-slip deformation along reactivated normal faults in Quaternary travertine deposits, Denizli Basin, western Turkey: Tectonophysics, v. 588, p. 154–170.

Vázquez-Urbez, M., Arenas, C., and Pardo, G., 2012, A sedimentary facies model for stepped, fluvial tufa system in the Iberian Range (Spain): the Quaternary Piedra and Mesa valleys: Sedimentology, v. 59, p. 502-526.

Viles, H.A., and Pentecost, A., 1999, Geomorphological controls on tufa deposition at Nash Brook, South Wales, United Kingdom: Cave and Karst Science, v. 26, p. 61–68.

Wang, E., Kirby, E., Furlong, K.P., van Soest, M., Xu, G., Shi, X., Kamp P.J.J., and Hodges, K.V., 2012, Two-phase growth of high topography in eastern Tibet during the Cenozoic: Nature Geoscience, v. 5, p. 640-645.

Winsborough, B.M., and Golubic, S., 1987, The role of diatoms in stromatolite growth: two examples from modern freshwater settings: Journal of Phycology, v. 23, p. 195–201.

Wischnewski, J., Mischke, S., Wang, Y.B., and Herzschuh, U., 2011, Reconstructing climate variability on the northeastern Tibetan Plateau since the last Late glacial – a multi-proxy, dual-site approach comparing terrestrial and aquatic signals: Quaternary Science Review, v. 30, p. 82–97.

Wright, J.S., 2000, Tufa accumulations in ephemeral streams: observations from the Kimberley, north-west Australia: Australian Geographer, v. 31, p. 333–347.

Zentmyer, R., Myrow, P.M., and Newell, D.L., 2008, Travertine deposits from along the South Tibetan Fault System near Nyalam, Tibet: Geological Magazine, v. 145, p. 1-13.

Zhang, J., Wang, H., Liu, Z., An, D., and Dreybrodt, W., 2012, Spatial-temporal variations of travertine deposition rates and their controlling factors in Huanglong Ravine, China – a world's heritage site: Applied Geochemistry, v. 27, p. 211–222.

Figure captions

Fig. 1. Map of the travertine depositional settings in the Jiuzhaigou National Nature Reserve (Sichuan province of China) and geological sketch map of the watershed area (simplified after Guo et al. 2006). The lateral extent of the travertine depositional setting along the valleys is not to scale.

Fig. 2. Travertine depositional settings along the longitudinal profile of Rize and Shuzheng valleys. The vertical extent of the travertine facies is not to scale. Longitudinal profile, TDS and temperature data (September 2010) are modified from Florsheim et al. (2013)

Fig. 3. A) The slope of the Jialijiage spring travertine; B) clast-supported debris-flow deposits consisting of carbonate rock fragments cemented by gravitational cement made of stalactites and pillars near the Jialijiage spring; C) ostracod shell in life position in clotted micrite from the channel of the present-day Jialijiage spring; D) photomicrograph of the stalactitic gravitational columnar calcite crystals fanning away downward from the clast surfaces of a Carboniferous grainstone (top) from Part B; crossed polars; C) isopachous cement around carbonate clasts and horizontal calcite rafts from the lower part of the deposit illustrated in Part B; D) the laminated appearance of the recent spring travertine of Part B); E) photomicrograph of the spring travertine of Part D, showing seasonal columnar calcite alternating with smaller crystals; some of the crystals have a micrite rim; crossed polars.

Fig. 4. A) The vegetated pool and dam system seen from Shuzheng looking downstream; B) small pool and dam system (secondary dams) downstream of Panda lake; floating leaves and wood debris are trapped at the upper rim of the dams and become actively encrusted by travertine; C) recent leaf casts preserved in the travertine on the top margin of a secondary dam downstream of Nuorilang waterfall; D) photomicrograph of the travertine of Part C; leaves and algae are encrusted by clotted micrite and microspar.

Fig. 5. A) The area of strong-turbulence water flow at Pearl shoal dominated by bare travertine crust; B) The area of weak- turbulence water flow at Pearl shoal, dominated by plants, macrophytes, algae and moss; C) the upper surface of the bare travertine crust sampled in the area of strong-turbulence water flow at Pearl shoal; D) the upper surface of the travertine crust colonized by algae and moss, sampled in the area of weak-turbulence water flow at Pearl shoal; E) the vertical section of the bare travertine crust from the strong-turbulence water flow at Pearl shoal; F) the vertical section of the travertine crust colonized by algae and moss from the weak-turbulence water flow at Pearl shoal.

Fig. 6. A) Photomicrograph of highly porous clotted micrite incrustation of moss and algae and an ostracod shell in a vertical section of the travertine crust colonized by algae and moss from the area of weak-turbulence water flow at Pearl shoal (Fig. 4F); crossed polars; B) photomicrograph of vertical calcite crystals arranged in dense laminae including erected parallel filaments of *Phormidium* and nearly vertical cyanobacterial “bush” fabrics and radiating bundles of *Phormidium* sp. arranged in shrub-like structures (lower left); the cyanobacterial-filaments-rich facies is capped by more porous algal layers consisting of *Oocardium stratum*; vertical section of the bare travertine crust from the area of strong-turbulence water flow at Pearl shoal (Fig. 4E); crossed polars; C) photomicrograph of the *Oocardium stratum* facies in the bare travertine crust from the area of strong-turbulence water flow at Pearl shoal (Fig. 4E); the large, branched, bush-shaped calcite biocrystals are originally centered by a hollow tube which was occupied by the *Oocardium* unicells during growth; crossed polars; D) photomicrograph of the *Oocardium stratum* facies containing algal filaments of probable *Vaucheria* asymmetrically encrusted with radial platy calcite crystals (at center); crossed polars.

Fig. 7. A) The plastic plate placed in shallow water at the margin of the turbulent-water-flow zone at Pearl shoal encrusted by travertine after one year, from August 2010 to August 2011. B) photomicrograph of radial sparry calcite crystals with sparse *Phormidium* filaments in the crust of Part A; natural light (above) and crossed polars (below); C) SEM top view of the upper surface of the crust of Part A, showing the radiating calcite bundles with attached stalked diatoms; D) SEM cross-section view of the crust deposited in one year; notice that the diatoms are engulfed into the

crust and were not nucleation points for the growth of the calcite crystals; E) SEM view of the travertine crust formed on the lower surface of the plate of Part A, showing the dramatic concentration of diatoms partially enclosed in EPS; F) SEM view of the travertine crust formed on the lower surface of the plate of Part A, with large diatom frustules; the hole in the crust were formerly occupied by cyanobacterial filaments.

Fig. 8. A) The spectacular waterfall downstream of Pearl Shoal. Note the protruding hanging wall covered by moss and the large collapsed blocks at the foot of the cliff; B) molds of logs and branches covered by travertine at the core of a dry waterfall downstream of Swan lake; C) porous moss cushion protruding from a vertical waterfall wall as it became encrusted by carbonate; the sponge-like carbonate sediment retains the shape of the moss that has been rapidly fossilized; dry waterfall downstream of Swan lake; D) moss stems actively encrusted by travertine on the vertical wall of the Jialijiage spring system (Fig. 2A); E) photomicrograph of the fossilized moss cushion of Part C, the original stems, now appearing as empty cavities (black), were encrusted by microspar and clotted micrite; crossed polars; F) densely packed larval tubes on the vertical wall of dry waterfall downstream of Swan lake; G) photomicrograph of hollow larval tubes covering clotted micrite and *Oocardium* travertine; crossed polars.

Fig. 9. A) Speleothems in dry shield cave (right) formed by the progradation of an old waterfall toward the left by encrustation of moss cushions; dry waterfall downstream of Swan lake; B) photomicrograph of moss encrusted by layered clotted micrite in turn covered by trigonal and blocky calcite crystals; crossed polars; C) photomicrograph of trigonal calcite crystals radiating from a clotted micrite surface (left); crossed polars; D) laminar travertine facies partially cut by dissolution features marked by a red residue; note the columnar growth of the laminae; crossed polars; E) SEM view of interlocking trigonal calcite crystals; F) SEM close-up view of one trigonal calcite crystal of Part E; note the tapered crystal termination.

Fig. 10. A) Dry riverbed covered by fluvial crust downstream of Panda waterfall; note the large number of logs encrusted by travertine (April 2015); the water flow is completely intercepted by a system of sinkholes located about one kilometer upstream; B) The Panda waterfall completely dry, December 2015; note the long ice stalactites attached to the hanging wall of the waterfall, adding considerable weight to the waterfall rim, which periodically collapses as demonstrated by the large volume of debris at the foot of the waterfall; C) The Panda waterfall during the flood season, August 2012; note the protruding hanging wall and the large amount of collapsed debris at the foot of the waterfall; D) photomicrograph of sand travertine debris collected in the riverbed downstream of Swan lake; the grains consist of clotted micrite, coated sparry calcite, and limestone fragments; crossed polars; E) travertine chips and sand ripples in the riverbed downstream of the Panda waterfall; the fragments are produced by the exposure and degradation of the of older travertine crusts in the riverbed and margins during the dry season from December to May.

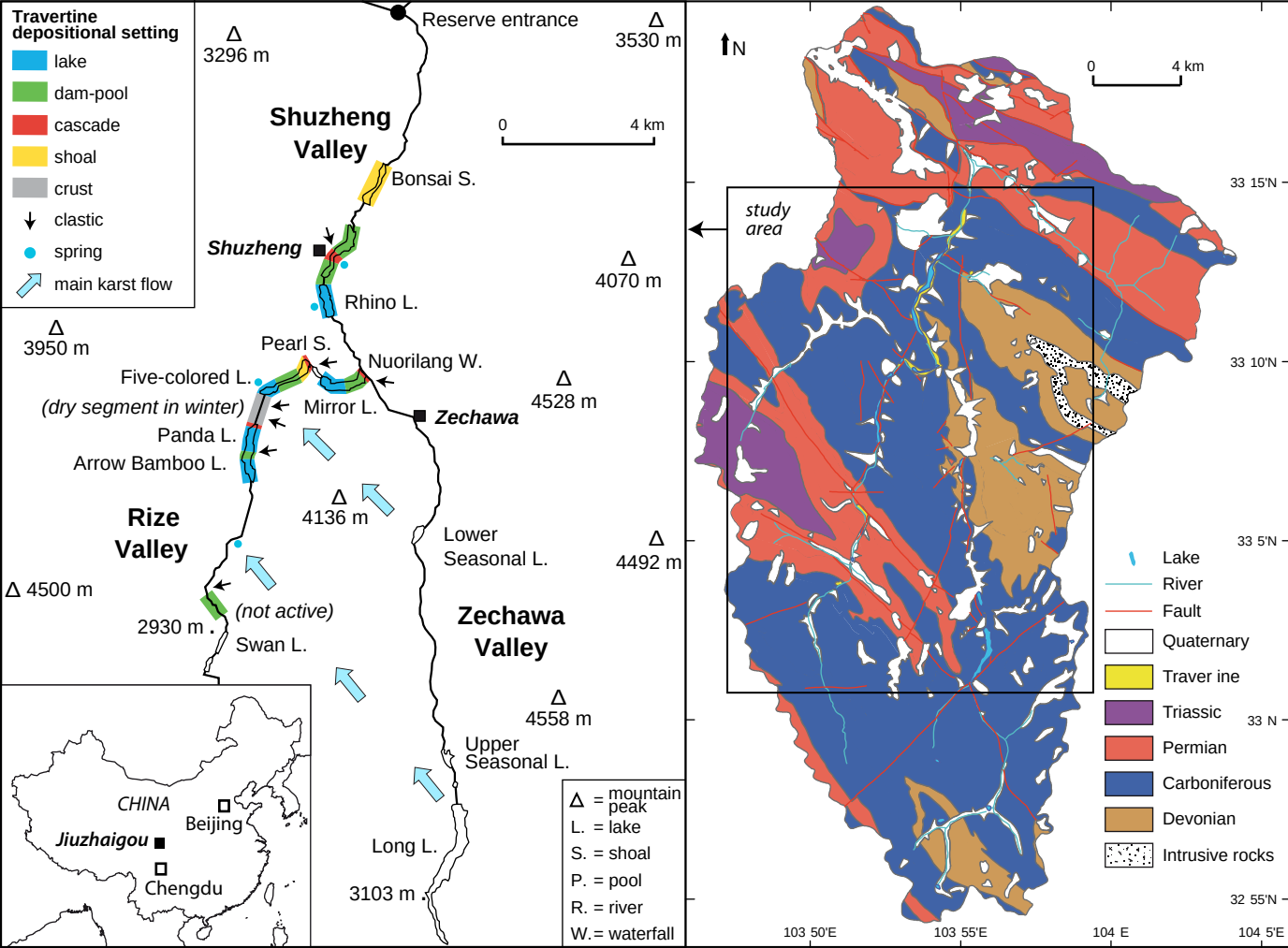
Travertine depositional setting
lake
dam-pool
cascade
shoal
crust
clastic
spring
main karst flow
Reserve entrance
Δ 3530 m
Δ 3296 m
Shuzheng Valley
0 4 km
Bonsai S.
Shuzheng
Rhino L.
Δ 4070 m
Δ 3950 m
Pearl S.
Nuorilang W.
Five-colored L.
(dry segment in winter)
Mirror L.
Zechawa
Δ 4528 m
Panda L.
Arrow Bamboo L.
Rize Valley
Δ 4136 m
Lower Seasonal L.
Δ 4492 m
Δ 4500 m
2930 m
(not active)
Swan L.
Zechawa Valley
Δ 4558 m
Upper Seasonal L.
CHINA
Beijing
Jiuzhaigou
Chengdu
Long L.
3103 m
Δ = mountain peak
L. = lake
S. = shoal
P. = pool
R. = river
W.= waterfall
N
0 4 km
study area
33 15'N
33 10'N
33 5'N
33 N
32 55'N
103 50'E
103 55'E
104 E
104 5'E
Lake
River
Fault
Quaternary
Traver ine
Triassic
Permian
Carboniferous
Devonian
Intrusive rocks

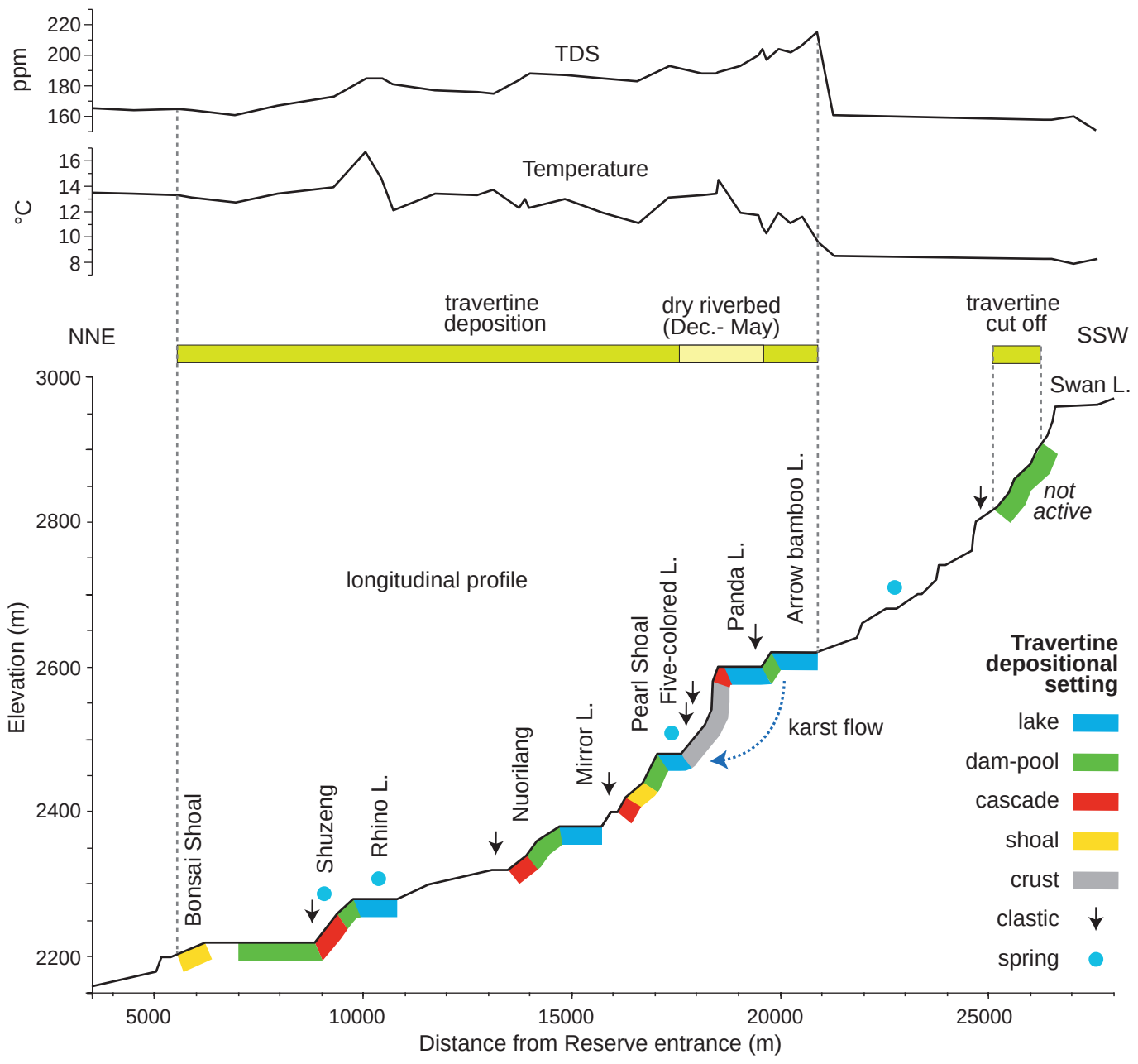
ppm
220
200
180
160
TDS
°C
16
14
12
10
8
Temperature
travertine deposition
dry riverbed (Dec.- May)
travertine cut off
NNE
SSW
Swan L.
not active
3000
2800
2600
2400
2200
Elevation (m)
longitudinal profile
Bonsai Shoal
Shuzeng
Rhino L.
Nuorilang
Mirror L.
Pearl Shoal
Five-colored L.
Panda L.
Arrow bamboo L.
karst flow
Travertine depositional setting
lake
dam-pool
cascade
shoal
crust
clastic
spring
5000
10000
15000
20000
25000
Distance from Reserve entrance (m)


A

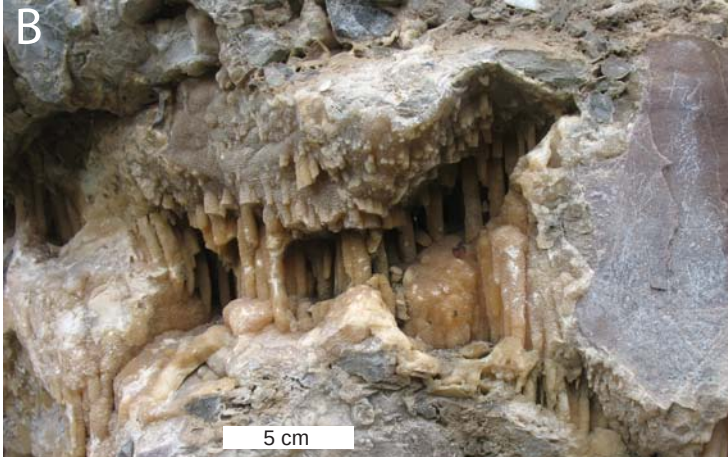
B
5 cm

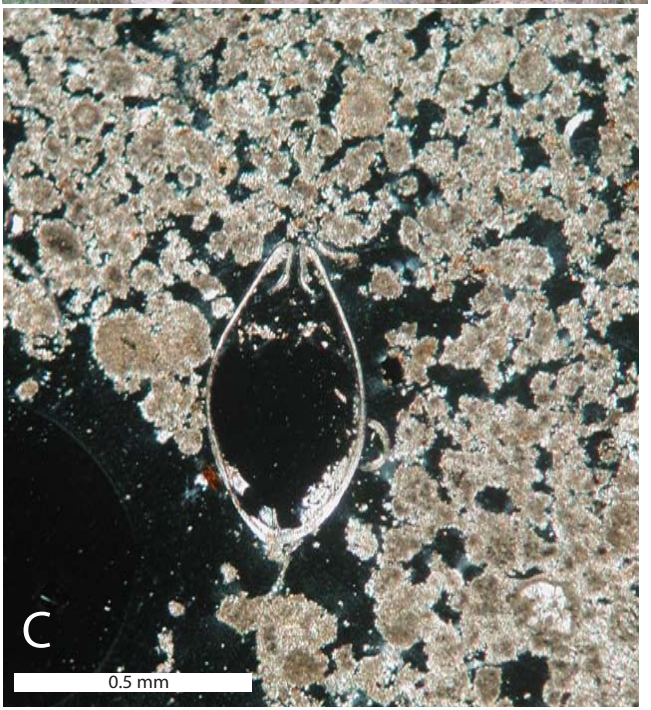
C
0.5 mm

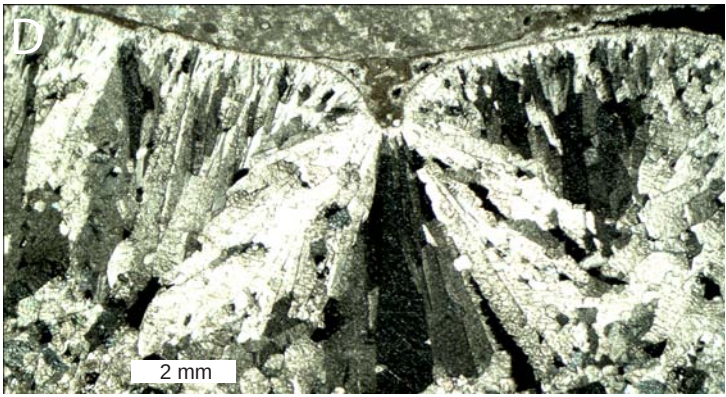
D
2 mm


E


F
1 cm


G
1 mm

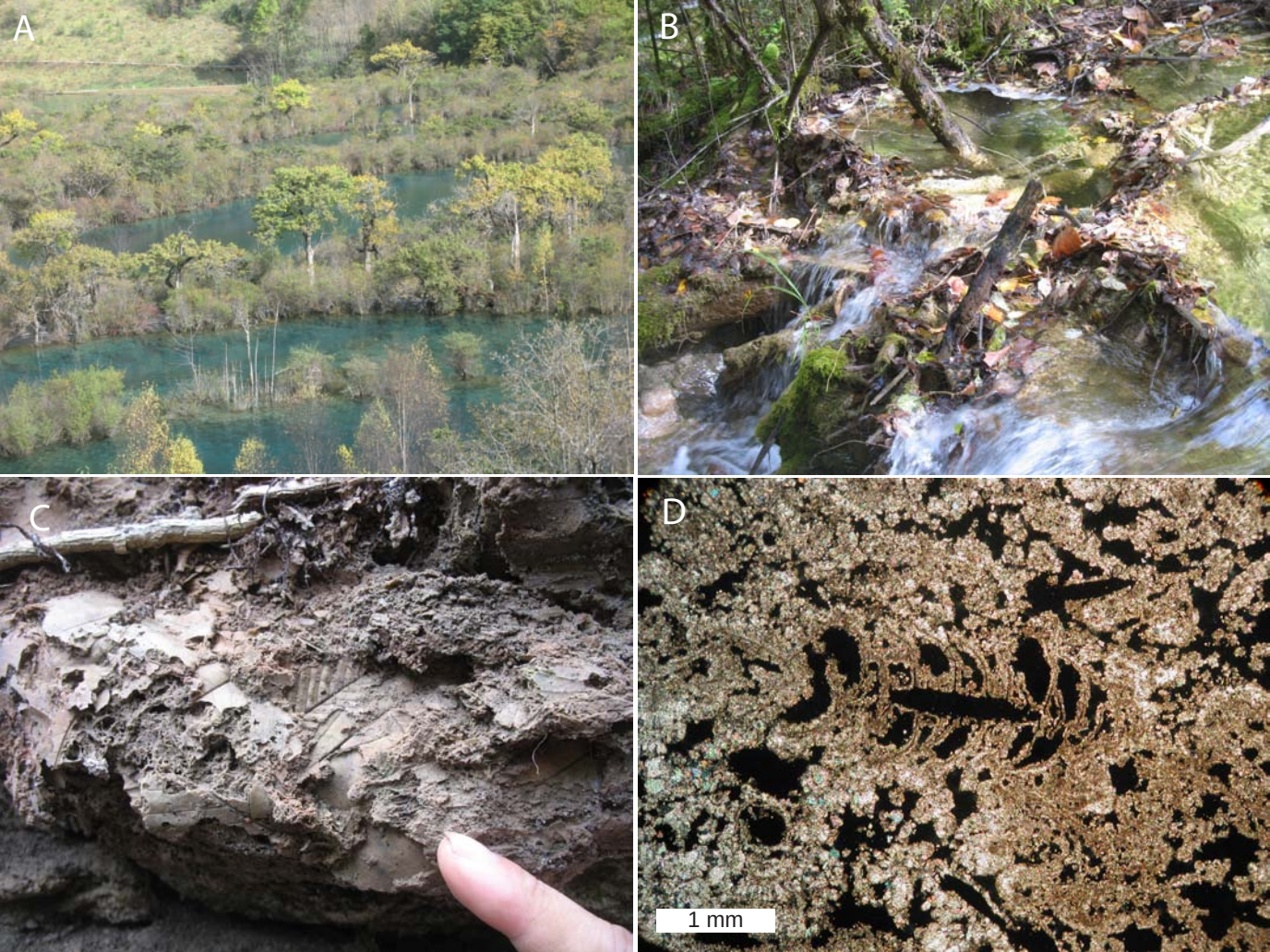
A
B
C
D
1 mm


A
B
1 cm
C
1 cm
D
E
1 cm
F
1 cm

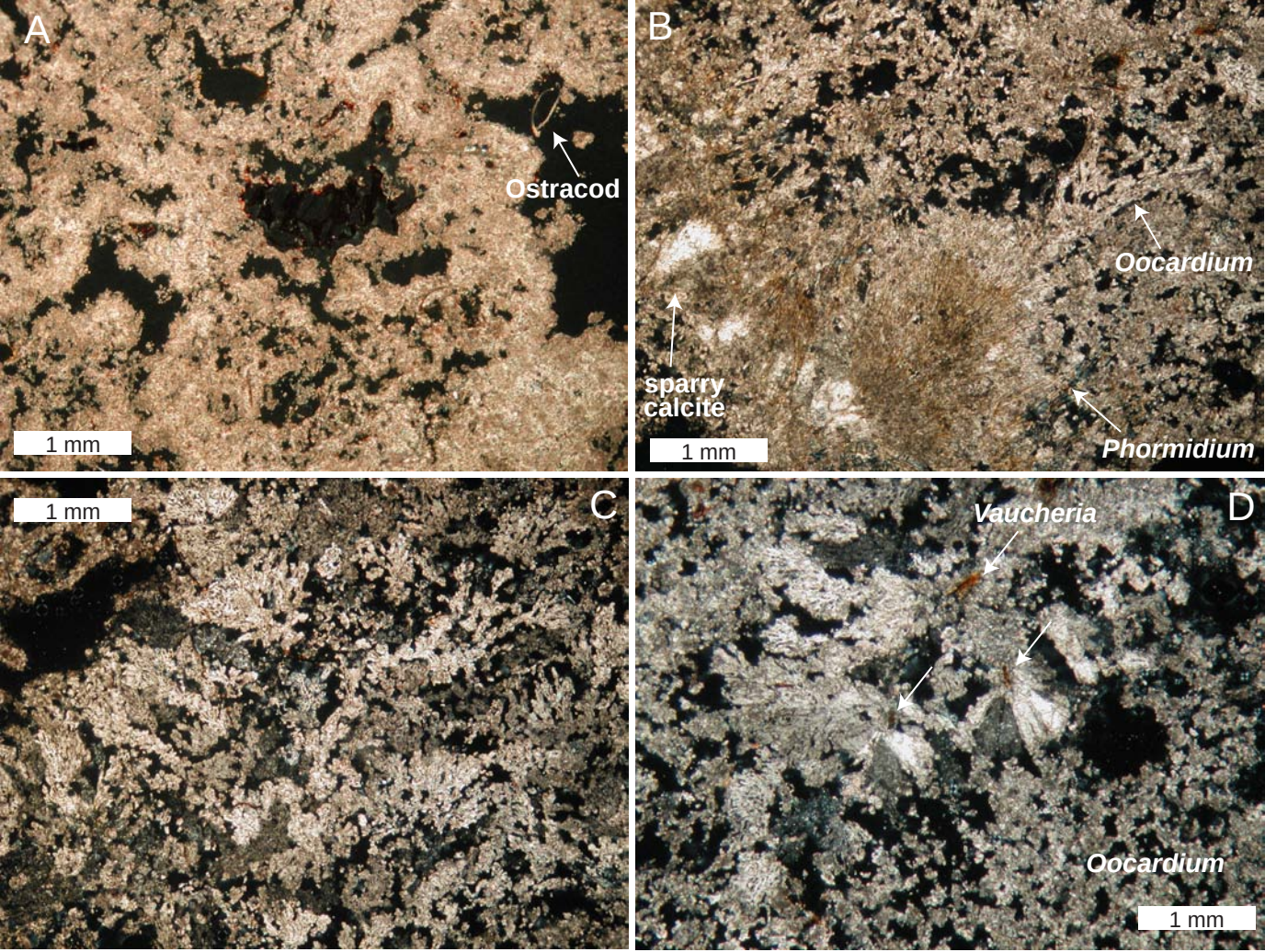
A
Ostracod
1 mm
B
Oocardium
sparry
calcite
1 mm
Phormidium
C
1 mm
D
Vaucheria
Oocardium
1 mm

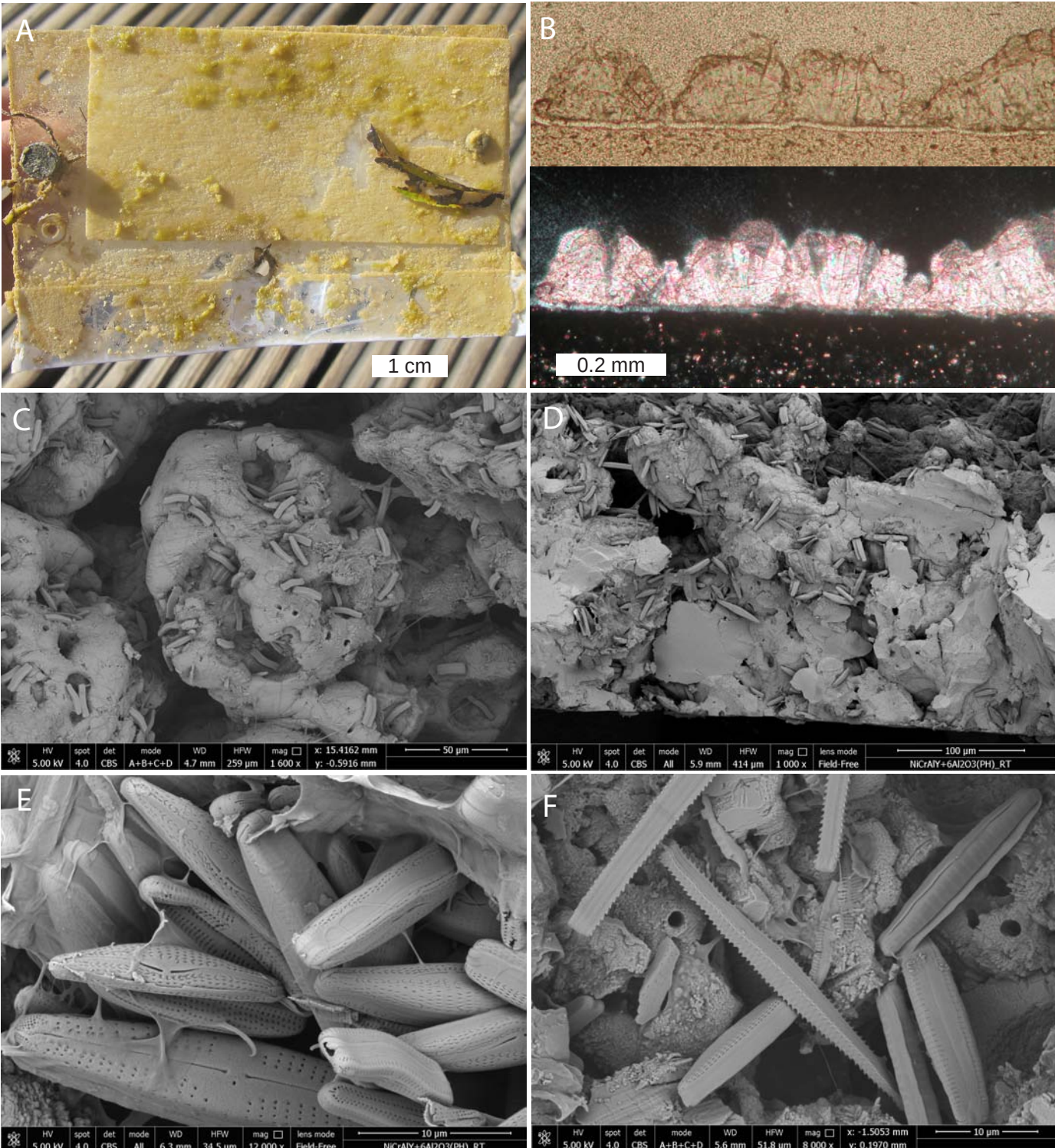
A
1 cm
B
0.2 mm
C
HV 5.00 kV | spot 4.0 | det CBS | mode A+B+C+D | WD 4.7 mm | HFW 259 µm | mag 1 600 x | x: 15.4162 mm y: -0.5916 mm | 50 µm
D
HV 5.00 kV | spot 4.0 | det CBS | mode All | WD 5.9 mm | HFW 414 µm | mag 1 000 x | lens mode Field-Free | 100 µm | NiCrAlY+6Al2O3(PH)_RT
E
10 µm
F
HV 5.00 kV | spot 4.0 | det CBS | mode A+B+C+D | WD 5.6 mm | HFW 51.8 µm | mag 8 000 x | x: -1.5053 mm y: 0.1970 mm | 10 µm


A


B


C

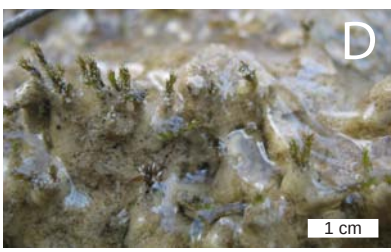
D
1 cm

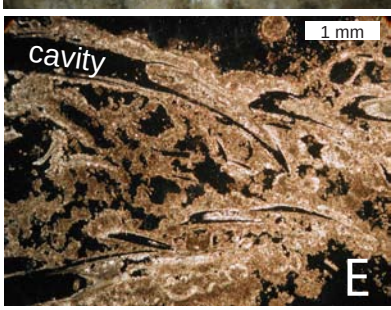
1 mm
cavity
E


F
1 cm

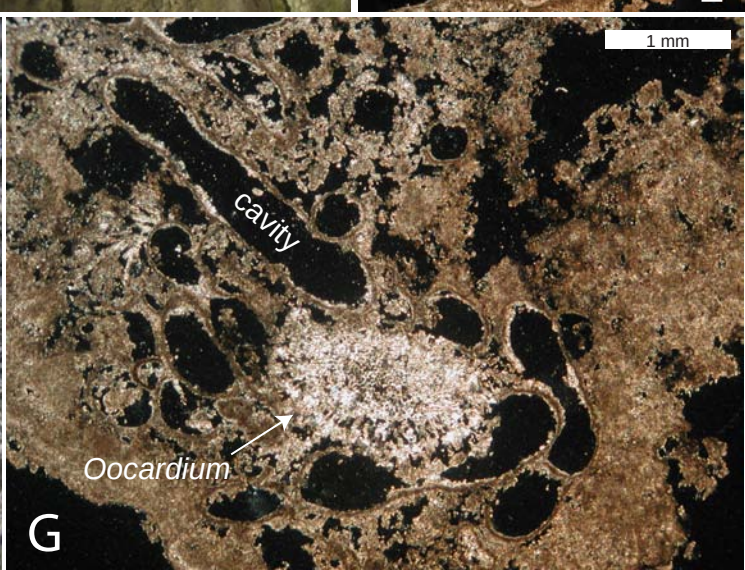
1 mm
cavity
Oocardium
G

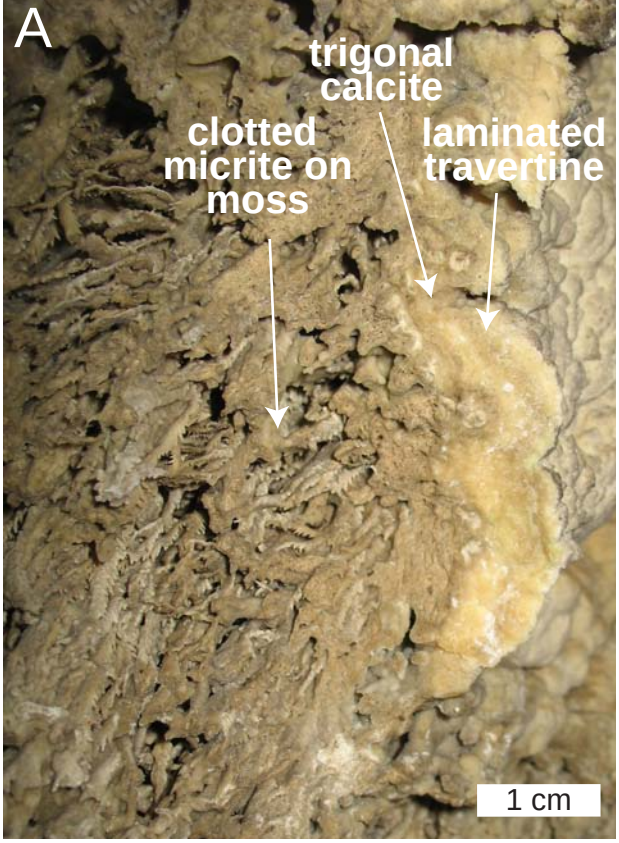
A
trigonal calcite
clotted micrite on moss
laminated travertine
1 cm

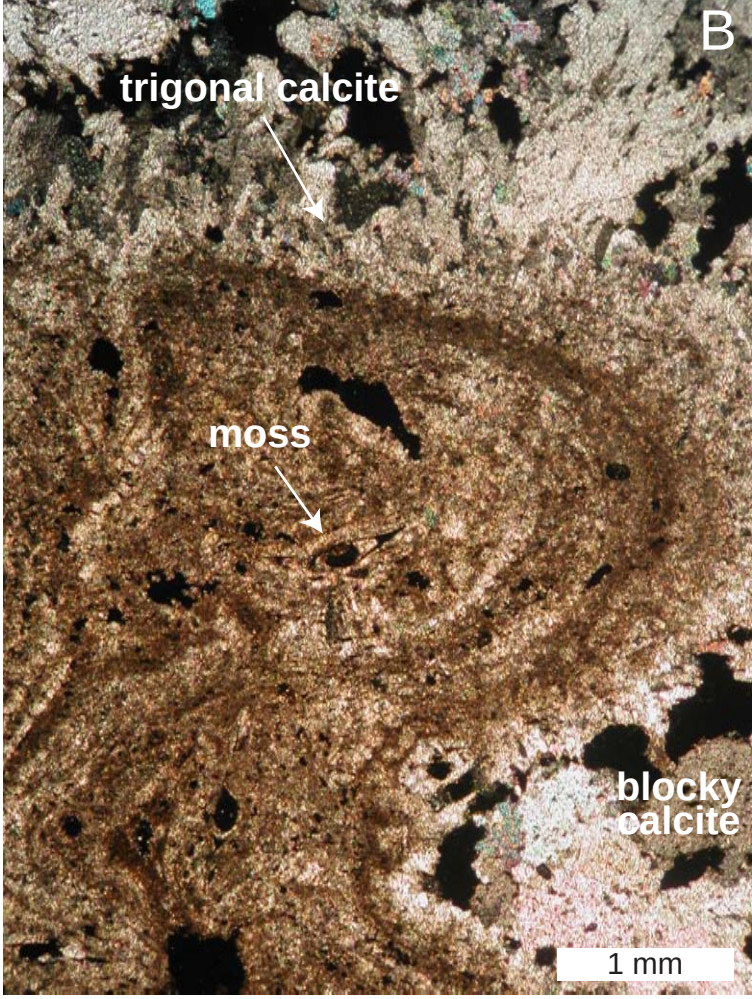
B
trigonal calcite
moss
blocky calcite
1 mm


C
1 mm


D
1 mm

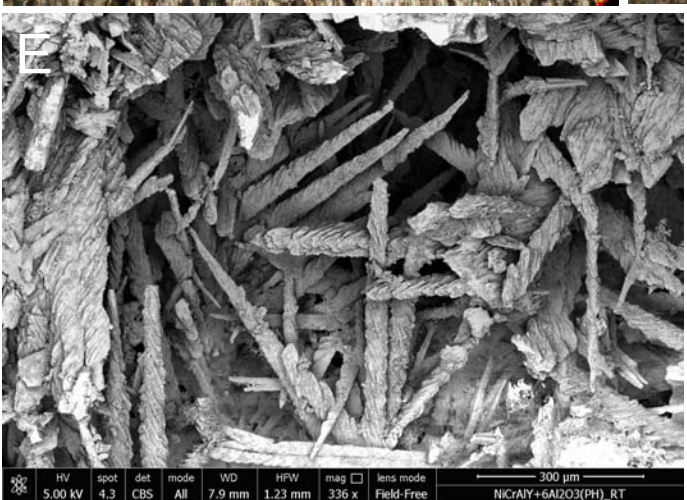
E
HV 5.00 kV
spot 4.3
det CBS
mode All
WD 7.9 mm
HFW 1.23 mm
mag 336 x
lens mode Field-Free
300 µm
NiCrAlY+6Al2O3(PH)_RT

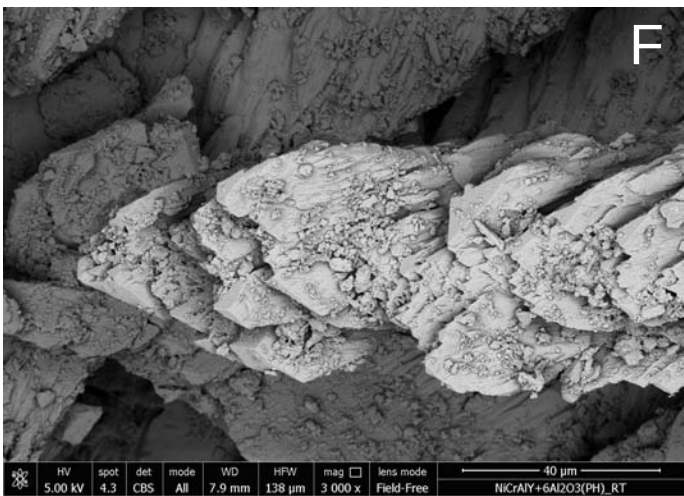
F
HV 5.00 kV
spot 4.3
det CBS
mode All
WD 7.9 mm
HFW 138 µm
mag 3 000 x
lens mode Field-Free
40 µm
NiCrAlY+6Al2O3(PH)_RT


A


B


C

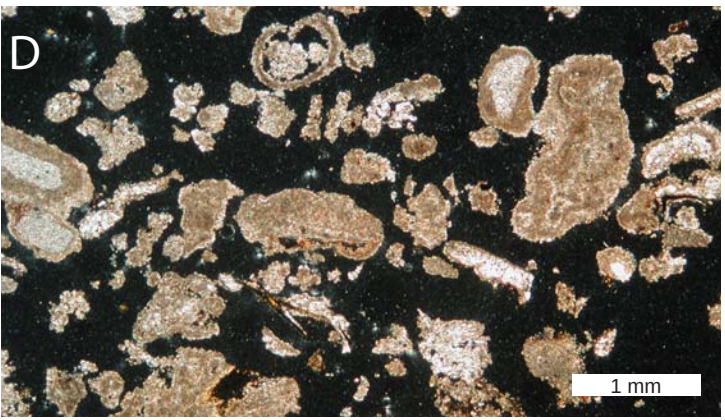
D
1 mm

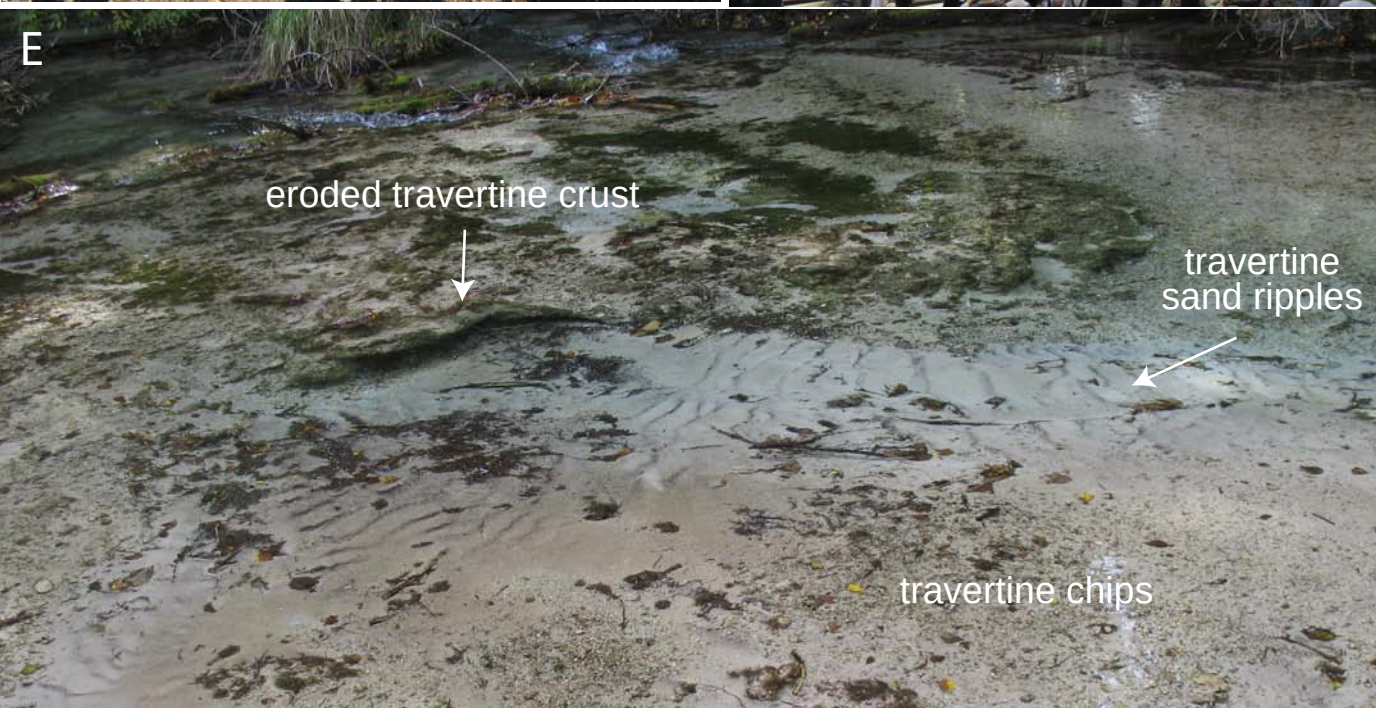
E
eroded travertine crust
travertine
sand ripples
travertine chips